Field Energy Performance of an Insulating Concrete Form (ICF) Wall

W. Maref, M. M. Armstrong, H. Saber, M. Rousseau, G. Ganapathy, M. Nicholls and M.C. Swinton

IRC-RR-326

March 2012

National Research Council Canada
Conseil national de recherches Canada

Canada

Acknowledgements

The authors wish to thank Mr. Silvio Plescia at the Canada Mortgage and Housing Corporation (CMHC) and Mr. Anil Parekh at Natural Resources Canada (NRCan) for contributing funding for this project and NRC for providing the funding to enable researchers to build, operate and maintain a state-of-the-art Field Exposure of Walls facility.

Our thanks are also extended to Ross Monsour at Ready Mix Concrete Association of Ontario (RMCAO) for his contribution in providing the test specimens.

Disclaimer

This Project was partially funded by Canada Mortgage and Housing Corporation (CMHC) under Part IX of the National Housing Act, however the analysis, Interpretations and recommendations expressed in this report are those exclusively offered by the National Research Council Canada, Institute for Research in Construction. CMHC assumes no liability for any damage, injury, expense or loss that may result from the use of this report, particularly, the extrapolation of the results to specific situations or buildings.

Executive Summary

The National Research Council of Canada's Institute for Research in Construction (NRC-IRC) in collaboration with Canada Mortgage and Housing Corporation (CMHC) and Natural Resources Canada (NRCan) evaluated the dynamic heat transmission characteristics through two identical Insulating Concrete Form (ICF) wall assemblies. The ICF specimens were provided by an industry partner – the Ready Mixed Concrete Association of Ontario (RCMAO). The walls were exposed to naturally occurring climate at the in the NRC-IRC Field Exposure of Walls (FEWF) test facility in Ottawa, Canada from 13-Oct-09 to 16-Sep-10.

Heat flux and temperature data was collected from both of the wall assemblies. However, the results from one wall assembly only (Wall 1) were chosen for detailed analysis, due to suspected interior overheating of Wall 2 and potentially erroneous heat flux data. Error in heat flux data was discovered through comparison of measured data with results from the hygrothermal model *hyg*IRC-C (Saber, 2011).

The ICF wall had a measured pseudo-steady state R-value of RSI 3.77 [R21.4]. Additionally, correlations between the temperature at the exterior surface of the ICF and the exterior surface of the concrete revealed a buffering effect of approximately 5 days due to the mass of the ICF.

Measured 15-minute heat flux data from Wall 1 were compared to the expected heat flux through a theoretical wall with identical steady-state R-value (RSI 3.77 [R21.4]) and no mass effect. This analysis showed that the ICF moderated heat loss to and from the interior. The interior heat flux through the wall was not following weather changes on the outside instantaneously. This was interpreted as the buffering effect of the mass. The measured heating season peak in heat flux leaving the room was 8.3 W/m^2, below the expected peak in heat flux without mass effect of 10.3 W/m^2. The peak heat flux entering the room in summer was also reduced by the mass effect of the ICF, 2.2 W/m^2, as opposed to an expected 5.6 W/m^2 for a wall with no mass effect. This may have implications for the sizing of heating and cooling equipment.

Some seasonal storage effects were apparent. When the mass of the concrete was cooling (from September to December) heat losses from the room to the ICF were slightly lower than the expected heat losses for a wall with no mass effect. When the mass of the concrete was warming up (February to June), heat losses from the room to the ICF were slightly higher than would be expected without mass effect. This seasonal effect was small compared to the impact of the mass on peak heat losses and gains.

The results from this experiment are limited to a single wall section and set of conditions. Modeling is suggested to further explore the optimization of ICF insulation thickness for different wall orientations and climate. Whole house modeling would be required to explore the dynamic interaction of ICF's with solar gains and to quantify the impact of the ICF mass on annual energy consumption.

Table of Contents

1 Introduction 1
2 Objectives 2
3 Methodology 3
3.1 Construction 3
3.2 Instrumentation 5
3.3 Material Properties Affecting the Thermal Response of Wall Systems 6
4 Results 8
4.1 Outdoor Air Temperature 8
4.2 Indoor Air Temperature 9
4.3 Surface Temperature 10
4.3.1 Winter Surface Temperature 11
4.3.2 Summer Surface Temperature 12
4.3.3 Relationship between Concrete Exterior Surface Temperature and ICF Exterior Surface Temperature 13
4.4 Heat Flux 15
4.5 Pseudo Steady State R-value 18
4.6 Heat absorbed and released by the concrete 19
4.7 Impact of mass on heat flux 20
4.7.1 Monthly heat loss and gain 23
4.7.2 Monthly maximum and minimum heat flux 27
5 Wall 1 compared to Wall 2 29
5.1 Difference in Interior Temperature 29
5.2 Difference in Heat Flux 31
6 Conclusions 33
7 References 34
Appendix A - ICF Construction 36

List of Figures

Figure 1. View of the ICF wall specimens before installation of siding 3
Figure 2. ICF wall vertical cross section 4
Figure 3. Elevation view from the interior of one ICF wall 5
Figure 4. Removed section of EPS foam for heat flux transducer installation 6
Figure 5. Heat flux transducer repositioned in the middle of the EPS 6
Figure 6. Outdoor Air Temperature, from the Ottawa International Airport (Environment Canada, 2010) 8
Figure 7. Chamber Air Temperature, as measured by an RH&T sensor adjacent to the interior surface of Wall 1 9
Figure 8. Measured 15-minute temperature data 10
Figure 9. Winter detail of measured 15-minute temperature data 11
Figure 10. Summer detail of measured 15-minute temperature data 12
Figure 11. Average daily concrete exterior surface temperature vs. average daily ICF exterior surface temperature 13
Figure 12. Average daily concrete exterior surface temperature vs. 5-day moving average of ICF exterior surface temperature 14
Figure 13. Average daily concrete exterior surface temperature and 5-day moving average of ICF exterior surface temperature 14
Figure 14. Heat flux at the interior and the exterior of the ICF (15-minute data) 15
Figure 15. Detail of winter heat flux at the interior and the exterior of the ICF (15-minute data) 16
Figure 16. Detail of summer heat flux at the interior and the exterior of the ICF (15-minute data) 17
Figure 17. Example of occasions where the ICF wall is in “Pseudo Steady State” 18
Figure 18. Pseudo Steady state R-value for the ICF 19
Figure 19. Daily heat absorbed and released by the concrete 20
Figure 20. Heat flux at the interior surface of the ICF, with and without mass (15-minute timestep) 21
Figure 21. February detail of heat flux at the interior surface of the ICF, with and without mass (15-minute timestep) 22
Figure 22. February detail of heat flux at the interior surface of the ICF, with and without mass (15-minute timestep) 22
Figure 23- Monthly comparison of heat loss through an ICF wall and a wall with no mass. 25
Figure 24- Cumulative energy loss for walls with and without mass (heating season only). 25
Figure 25. Monthly comparison of heat gain through the ICF, and a wall without mass 26
Figure 26 - Cumulative energy gain for walls with and without mass. 26
Figure 27. Monthly comparison of 15-minute heat flux through the ICF and a wall with no mass. (Each point represents the average monthly heat flux, with the bars indicating the monthly maximum and minimum heat flux values.) 27
Figure 28. Comparison of Wall 1 and Wall 2 temperature measurements 30
Figure 29. Difference in the ICF interior surface temperature for Wall 1 and Wall 2 30
Figure 30. Comparison of Wall 1 and Wall 2 measured Heat Flux at the Centre of the Interior EPS Foam (HF3). Each point represents the average monthly heat flux, with the bars indicating the monthly maximum and minimum heat flux values. 31
Figure 31. Comparison of the modeled heat flux and measured heat flux at location HFT3 for Wall 1. 32
Figure 32. Comparison of the modeled heat flux and measured heat flux at location HFT3 for Wall 2. 32

Figure A-1. Removal of trees from the FEWF site, allowing full west exposure to wind, rain and sun. 36
Figure A-2. Installation of a gravel pad to allow the forklift room to manoeuvre when lifting the ICF walls into place 36

Figure A-3. Assembling the insulating form inside the Research House. 37
Figure A-4. Three assembled insulating forms inside the Research House. Note: three ICF wall specimens were fabricated, although only two were installed for monitoring at the FEWF. The third wall was made as a backup, in case either of the other two wall specimens was damaged during installation. 38
Figure A-5. Thermocouples installed on the exterior and interior surfaces of the foam prior to pouring the concrete. 39
Figure A-6. Preparing the three insulating forms for the concrete pour. 39
Figure A-7. Steel rebar inserted into the ICF frame prior to pouring the concrete. 40
Figure A-8. Preparing the three insulating forms for the concrete pour. 40
Figure A-9. Preparing the three insulating forms for the concrete pour. 41
Figure A-10. Arrival of the concrete mixer and pumping truck. 41
Figure A-11. Pouring the concrete into the insulating form. 42
Figure A-12. Vibrating the concrete to remove air pockets. 42
Figure A-13. Water pooling at the base of the ICF wall specimen after pouring the concrete. 43
Figure A-14. Water pooling at the base of the ICF wall specimen after pouring the concrete. 43
Figure A-15. Wooded alignment jig with threaded rods for the forklift lifting points. 44
Figure A-16. The alignment jig holds the metal rods in place while the concrete cures. 44
Figure A-17. Once the concrete was cured, the wooded jig was removed, extensions were added to the threaded rods, and metal plates were attached to provide lifting points for the forklift. 45
Figure A-18. Preparing the FEWF opening for ICF wall installation. 46
Figure A-19. Preparing the FEWF opening for ICF wall installation. 46
Figure A-20. Lifting the first ICF wall into position. 47
Figure A-21. Lifting the first ICF wall into position. 47
Figure A-22. The ICF is separated from the framing by 4 inches of EPS foam on the sides, bottom and top (not shown). 48
Figure A-23. View of the bottom of the second ICF wall specimen as it is being lifted into position. 48
Figure A-24. Lifting the second ICF wall specimen into position. 49
Figure A-25. Lifting the second ICF wall specimen into position. 49
Figure A-26. Securing the second ICF wall specimen. 50
Figure A-27. Securing the second ICF wall specimen. Temporary vertical wood straps help guide the ICF wall specimen into place in the FEWF opening. 50
Figure A-28. ICF wall specimens installed in the FEWF opening. 51
Figure A-29. Metal L brackets hold the framing in place on either side of the ICF. 51
Figure A-30. Metal L brackets hold the framing in place on either side of the ICF. 52
Figure A-31. Metal L brackets hold the framing in place on either side of the ICF. 52
Figure A-32. Bolts secure the ICF wall specimen to the wood framing (2 bolts on each side). 53
Figure A-33. Instrumentation installed on the exterior of the walls, wires run to the chase between the two ICF specimens. 54
Figure A-34. OSB sheathing board installed around the specimens, joints sealed with sheathing tape. 54
Figure A-35. Sheathing membrane installed over the sheathing board, and cut to expose the face of the ICF walls. Sheathing membrane taped to the ICF on all four sides (shown in subsequent figures). 55
Figure A-36. Gaps in the ICF foam filled with low expansion polyurethane foam. A temporary sheathing membrane skirt prevents foam from adhering to the permanent sheathing membrane. 55
Figure A-37. Gaps in the ICF foam filled with low expansion polyurethane foam. A temporary sheathing membrane skirt prevents foam from adhering to the permanent sheathing membrane. 56
Figure A-38. Excess foam trimmed from the face of the ICF once cured, with the temporary skirt removed. 56
Figure A-39. Installation of vinyl siding over the entire FEWF opening. 57
Figure A-40. Detail view of instrumentation behind the vinyl siding – including: a heat flux transducer (round disk), pressure tap (clear plastic tube), and RH&T sensor (black sensor). 57
Figure A-41. Gaps in the ICF foam filled with low expansion polyurethane foam. Once cured, excess foam was trimmed from the interior face of the ICF. 58

Figure A-42. Instrumentation secured to the interior face of the ICF wall..... 58
Figure A-43. Drywall being installed on the interior of the ICF wall specimens. A square access panel was cut in the centre of the drywall to allow access to the instrumentation (including heat flux transducers) on the surface of the ICF. 59
Figure A-44. Wiring in the chase between the ICF walls leads to the basement. The holes for the wiring to pass through the base plate were sealed with foam..... 59
Figure A-45. The wiring chase was filled with glass fibre batt insulation, and sealed with a polyethylene air/vapour barrier. 60
Figure A-46. Tape seals the air/vapour barrier to the surrounding wall assembly. A ventilation duct passes through the wiring chase, to permit air conditioning of the test chamber during the cooling season. 60
Figure A-47. Installing drywall over the wiring chase between the ICF walls. 61
Figure A-48. Covering the seams and screw holes with drywall compound..... 62
Figure A-49. The seams and screw holes in the wall covered with drywall compound..... 62
Figure A-50. ICF walls painted with acrylic paint – with access panels open (the removed sections of drywall were set back into place and taped before the start of the experiment)..... 62
Figure A-51. The edges of the drywall were taped to the surrounding walls, floor and ceiling.... 63
Figure A-52. Installation of the interior climate control chamber..... 63
Figure A-53. Installation of the interior climate control chamber..... 64
Figure A-54. Removing a block of the EPS foam from the insulating form..... 65
Figure A-55. Removing a block of the EPS foam from the insulating form..... 65
Figure A-56. Replacing the foam block with a piece of wood for the concrete pour..... 66
Figure A-57. Filling the ridges of the foam blocks with concrete..... 66
Figure A-58. Filling the ridges of the foam blocks with concrete..... 67
Figure A-59. Curing the concrete in controlled conditions..... 67
Figure A-60. The foam blocks with cured concrete, prior to installation into the ICF walls. 68
Figure A-61. Cured ICF wall with removed foam block..... 68
Figure A-62. Positioning of a heat flux transducer on the surface of the concrete..... 69
Figure A-63. Re-installation of the foam block, with a second heat flux transducer installed on the outer surface of the EPS..... 69
Figure A-64. Removal of the heat flux transducer on the surface of the concrete, for repositioning. 70
Figure A-65. Foam blocks cut into two..... 70
Figure A-66. Repositioning of the heat flux centre between the two sections of the foam block. 71
Figure A-67. Installing the foam block back in the ICF wall..... 71
Figure A-68. Installing a second heat flux transducer on the interior surface of the ICF..... 72
Figure A-69. Sealing the edges of the foam block to the ICF with tape. 72
Figure A-70. Installation of the drywall access panel on top of the heat flux transducer, and repositioning of instrumentation (2 RH&T sensors and one pressure tap are shown). 73

List of Tables

Table 1. Dimension and thermal properties of the ICF components and glass fibre 7
Table 2. Average, Maximum and Minimum Monthly Outdoor Air Temperature..... 8
Table 3. Comparison of the Total Monthly Heat Gain and Losses at the interior of an ICF and an RSI 3.77 (R 21.4) wall with no mass. 24
Table 4. Comparison of the Maximum and Minimum Monthly Heat Flux at the interior of an ICF and an RSI 3.77 (R 21.4) wall with no mass..... 28

1 Introduction

Increasingly, home builders are turning towards a variety of construction methods to improve thermal performance while reducing the cost of construction. While Insulating Concrete Form (ICF) technology dates back to the late 1960s in Europe, ICF construction has only caught on in North America for use in residential and commercial construction over the last two decades (Hersh Servo AG, 2010). Generally modern ICFs consist of stackable formwork made of expanded polystyrene foam, which is filled on site with concrete, and then remains in place to provide permanent insulation. ICF technology offers the potential to improve air tightness and energy performance over the current practice of wood frame construction. With the growing presence of ICF construction in the market, it is important to gain an understanding of their actual performance in the field, and the role played by the thermal mass of the concrete in regulating heat losses.

A number of research projects have been performed on the thermal performance and thermal mass to investigate the potential of annual energy saving compared to traditional light-weight construction for example. The benefit of thermal mass was extensively investigated, especially at the Oak Ridge National Laboratory (Burch et al., 1984a, Burch et al., 1984b, Burch et al., 1984c, Christian, 1991, Kosny et al., 1998, Kosny et al., 2001, and Kossecka and Kosny, 1998). Petrie et al. (2001) conducted field investigation of two side-by-side houses in Knoxville, Tennessee. The two houses were similar except one house had Insulating Concrete Form (ICF) exterior walls and the other house had conventional wood-framed exterior walls. The results showed that the ICF house used 7.5% less energy than the conventional house. This work has shown that the principal benefit of thermal mass on thermal performance is to dampen fluctuations in interior conditions during significant fluctuations in outdoor conditions. Additionally, Petrie et al. (2001) conducted numerical simulations using DOE2 software to investigate the effect of different climates of six US cities (Phoenix, Minneapolis, Dallas, Boulder, Knoxville and Miami) on the energy consumption of both the ICF and conventional wood-framed houses. The results of cooling, heating and total electricity usage showed that the thermal mass had benefits for both cooling and heating. The ICF houses used 5.5% to 8.5% less energy annually than the conventional wood-framed houses. This range of saving (5.5% to 8.5%) agreed with Kosny's prediction of 4% to 10% savings with ICF houses compared to conventional wood-framed houses for 10 US climates (Kosny et al., 2001).

In 1999, NAHB Research Centre tested 3 side-by-side homes with floor area of 102 m^2 (1098 ft^2) to compare the energy performance of two ICF homes (one had an ICF plank system and one had an ICF block system) versus conventional wood-framed home (2x4 wall stud framing, sheathed with OSB, and insulated with fiberglass batt in the wall cavities). The three homes were located on the same street in Chestertown, Maryland. Also, the three homes had identical orientation, window area, roof construction, footprint, ductwork, and air handler systems. The testing was conducted over a one-year period beginning in April 1998. Heating consumption composed of two periods, April 1, 1998 through June 1, 1998 and October 6, 1998 through March 16, 1999. Cooling consumption represented the period from June 1, 1998 through September 22, 1998. This study showed that a 20% difference was noticed between ICF houses and the conventional wood-frame house's energy consumption. This difference can be attributed primarily to the higher effective R-value of the ICF walls and continuous insulation at the slab. The insulation for the walls of the ICF homes is R-20 while the wall insulation of the wood-framed home is R-13. The solid wall surfaces for all three homes make up approximately 44% of the total surface area of the homes (the remainder being made up of the ceiling area, windows, and doors). A 50% increase in the solid wall surface area resistance to conductive heat loss (R-20 compared to R-13) represented significant increased energy-efficiency. The foundation/slab details showed the impact clearly on the wood-frame home and was demonstrated greater heat loss in February and greater heat gain in August as evidenced by the wood-frame home's more pronounced and direct response to outdoor temperature changes. Given the total area and the thermal conductivity of

materials involved, the foundation/insulation/slab detail of the wood-frame home represented a significant source of heat loss and gain not evidenced in the ICF homes.

In 2001, the Portland Cement Association conducted a modeling study of the energy use of single-family houses with various exterior walls using DOE 2.1 software (Gajda, 2001). This study presented two ICF options: (1) concrete sandwiched by two insulation layers, and (2) insulation sandwiched by two concrete layers. The study examined the performance of eleven different types of exterior walls in 25 North American locations to determine the expected differences in energy use. In this study, the only differences for a given location were the exterior wall type and the capacity of the HVAC system. The results showed that houses with concrete walls had lower heating and cooling costs than walls with light construction, and contributed to additional savings through a reduction in the required heating and cooling system capacity.

In 2006, a project was conducted by Enermodal Engineering Limited for Canada Mortgage and Housing Corporation (CMHC) and the Ready Mix Concrete Associate of Ontario (RMCAO) to study the performance of a 7-storey insulating concrete form multi-residential building in Waterloo, Canada (Enermodal, 2006). Temperatures through the wall assembly were monitored at eight locations from December 1st, 2005 to February 26th, 2006. The project reported little contribution of the concrete to the steady-state R-value. During transient conditions, heat storage effects were reported. While the concrete never supplied heat to the interior during the winter monitoring period, the measured data showed that concrete did temper heat loss to the exterior during the periods of cold weather.

Recently, the National Research Council of Canada's Institute for Research in Construction (NRC-IRC) in collaboration with Canada Mortgage and Housing Corporation (CMHC) and Natural Resources Canada (NRCan) proposed evaluating the thermal response of two ICF wall assemblies in NRC-IRC's Field Exposure of Walls Facility (FEWF) for one year cycle of exposure to outdoor natural weathering conditions. The FEWF allows field monitoring of the thermal response of side-by-side test wall specimens exposed to natural weathering on the exterior and exposed to controlled indoor conditions.

2 Objectives

The National Research Council of Canada's Institute for Research in Construction (NRC-IRC) in collaboration with Canada Mortgage and Housing Corporation (CMHC) and Natural Resources Canada (NRCan) evaluated the dynamic heat transmission characteristics through two Insulating Concrete Form (ICF) wall assemblies in the NRC-IRC Field Exposure of Walls (FEWF) test facility for a one year cycle 2009-2010 of exposure to outdoor natural weathering conditions. The ICF specimens were provided by an industry partner – the Ready Mixed Concrete Association of Ontario (RCMAO). The scope of work included the design of the experiments, the installation of test specimens, the commissioning of the instrumentation, the operation of the test facility, the monitoring, data collection & analysis to determine the field energy performance of the ICF system. The objective of this project was to monitor the field performance of two ICF wall specimens for one year at the NRC Field Exposure of Wall Facility (FEWF), in order to understand and quantify the impact of the thermal mass of the concrete in the ICF wall system on heat losses and gains.

The objective of this study is also to use the present NRC-IRC' hygrothermal model called "hygIRC-C" used to interpret the readings of the instrumentations and to improve the experiment design by selecting the appropriate locations of instrumentation. Some results from this modelling study is presented in this report and detailed information can be found at Saber et al. (2011). Next, the present model is benchmarked by comparing its prediction against the test results. After gaining confidence in the simulation tool, it will be used to investigate the effect of

thermal mass of the concrete and EPS on the thermal response of the ICF assembly subjected to different Canadian climate conditions.

3 Methodology

Two identical ICF wall specimens were installed side by side in the FEWF test bay on the NRC Campus in Ottawa, Canada. The walls were located on the first floor of a two storey facility, with West exposure (Figure 1). A chamber provided controlled indoor conditions (~21°C, 30% humidity), and the walls were exposed to naturally occurring Ottawa climate (with an average of 4602 heating degree days <18°C (Environment Canada, 2010). Data was collected at 15-minute intervals from October 13th, 2009 to September 16th, 2010.

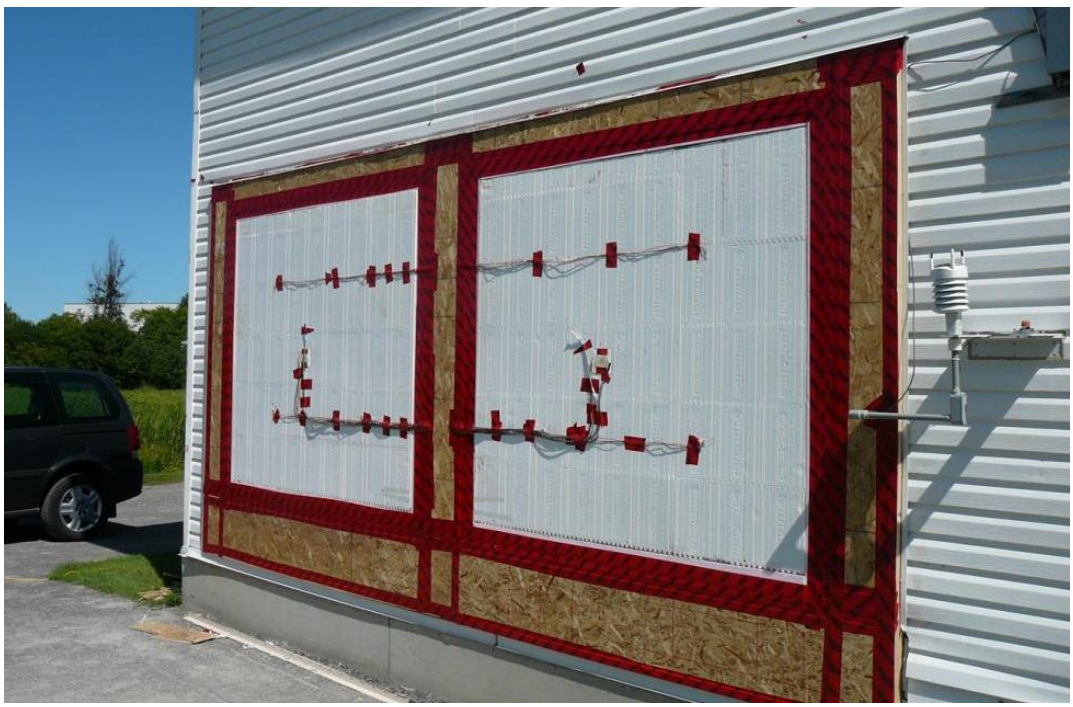

Figure 1. View of the ICF wall specimens before installation of siding

3.1 Construction

The ICF forms were assembled and thermocouples were installed on the interior of the form prior to pouring the concrete. The concrete was poured into the forms July 28th 2009, with the forms sitting outside the FEWF test bay. The specimens were allowed to cure outdoors (protected from direct precipitation) for 28 days before being lifted into place by forklift on August 25th 2009.

The ICF wall specimens measured 1828 x 1676 mm (71 15/16 x 66 in.) and featured 152 mm (6 in.) thick concrete surrounded by 64 mm (2.5 in.) of EPS foam on all sides, and 51 mm (2 in.) of EPS foam on the base (Figure 2). The ICF specimens were separated from surrounding construction by an additional 102 mm (4 in.) of XPS foam (Figure 3). This thickness of insulation was determined through simulation with *hyg*IRC-C. The thickness was chosen in order to prevent heat losses from the top, bottom and sides of the wall specimens, and for heat transfer to predominantly occur at the interior and exterior surfaces of the ICF. Chases 204 mm (6 in.)

wide were situated on either end of the test bay and between walls to provide space for running wires. The completed chases were filled with batt insulation. The finished walls included an interior drywall finish and exterior vinyl siding. Detailed documentation of the construction process is provided in Appendix A.

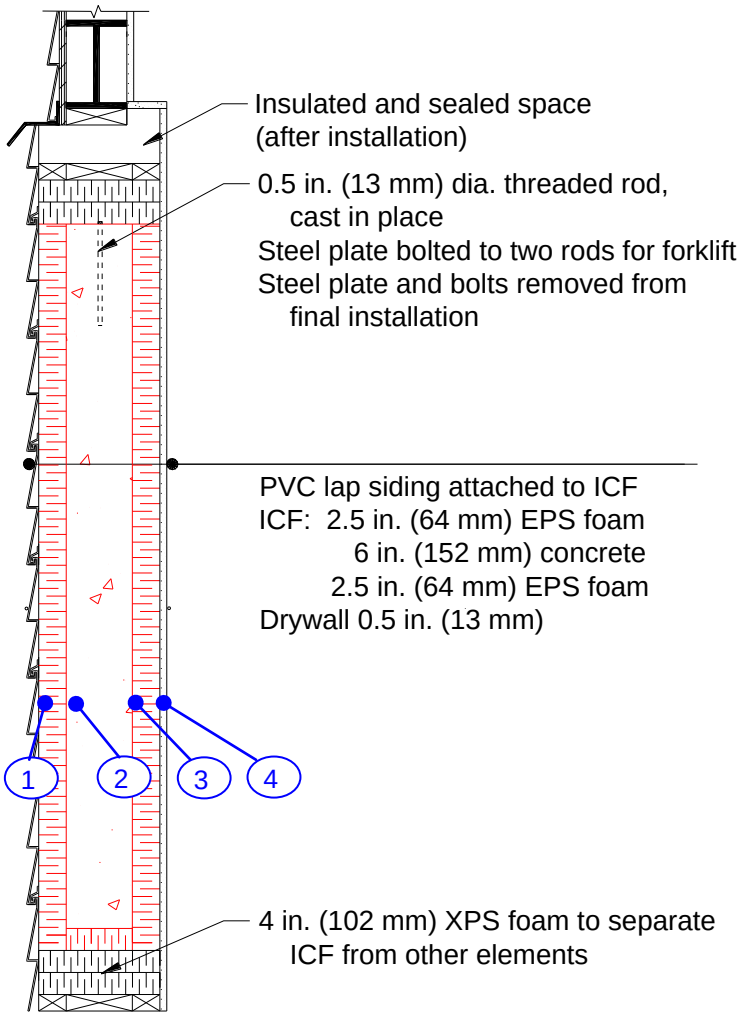

Figure 2. ICF wall vertical cross section

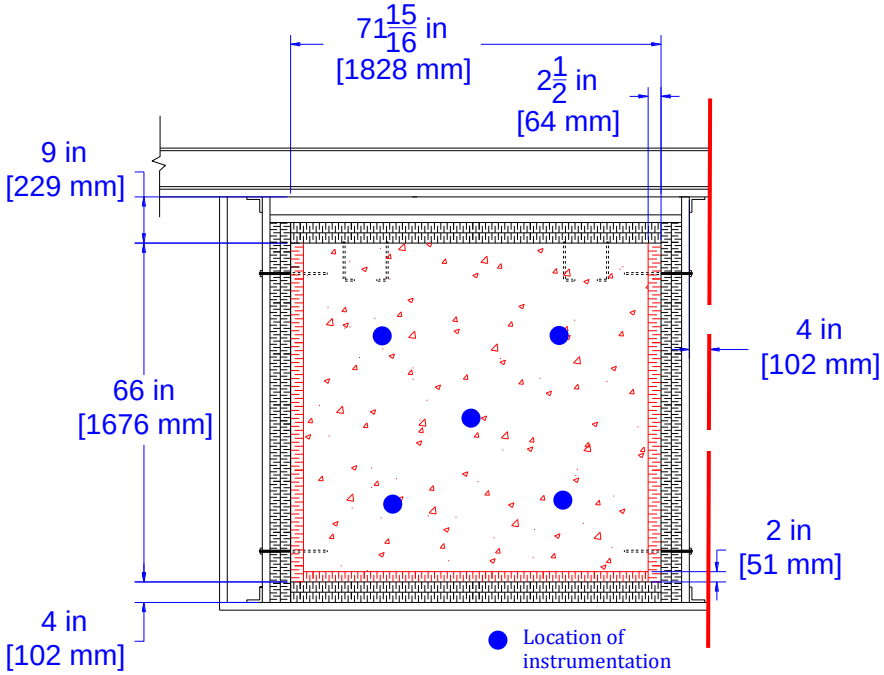

Figure 3. Elevation view from the interior of one ICF wall

3.2 Instrumentation

Instrumentation was located at four layers through each wall, as shown in Figure 2: 1) between the lap siding and the exterior EPS foam layer of the ICF; 2) on the face of the concrete behind the exterior EPS foam layer; 3) on the face of the concrete behind the interior EPS foam layer; and 4) between the drywall and the interior EPS foam layer of the ICF. At layers 2 and 3, two thermocouples were installed prior to pouring the concrete at each of the five instrumentation locations shown in Figure 3, for a total of 10 thermocouples per layer. Thermocouples were doubled at these locations as a precaution, in case damage to the sensors occurred during the pouring and curing of concrete. At layers 1 and 4, a total of four thermocouples were installed at all instrumentation locations except the bottom right location. The average temperature of each layer was used in this analysis and was obtained by averaging the readings of all thermocouples on each layer.

In each of the four layers, a single heat flux transducer was located at the central instrumentation location. This paper refers to the heat flux measured at location 2 (HF2) and location 3 (HF3) in the analysis. During the first few months of the experiment, HF2 and HF3 were positioned at the interface of the foam and the concrete. This proved a complex task due to the ridges on the interior side of the foam. To provide a flat surface for the heat flux transducers so that the measured heat flux component was perpendicular to the surface, sections of foam were removed prior to pouring the concrete. The ridges of the removed section were filled in with concrete and cured (Figure 4) before the foam section was put back into position. However, this meant that the heat flux transducer was not exposed to a uniform material – but rather alternating lines of foam and concrete on one side. This resulted in erroneous readings, based on those expected from the nominal R-value of the system. Simulation using *hyg*IRC-C was required to interpret the erroneous results and try to improve the experiment design by repositioning the heat flux transducers at critical locations to avoid the fin effect. A model was used to re-design and correct the location of the HFTs, and benchmarked later on. Numerical simulations were conducted to investigate the differences in the predicted heat fluxes at different locations in the foam (at the outer surface of the foam, middle of the foam and foam-concrete interface). The numerical results

showed that the differences caused by location were very small, and were approximately within the uncertainties of the heat flux transducers (Saber, 2010b). These small differences were due to the small thermal mass of the foam. Consequently, in order to expose the heat flux transducers to a uniform material, HF3 was repositioned on January 14th between two blocks of foam (Figure 5). The same correction was made to HF2 on January 29th. Thereafter, the predicted results from the simulation could be compared directly with the measured data. Temperature and heat flux data was sampled every minute, and the average was stored every 15-minutes.

Figure 4. Removed section of EPS foam for heat flux transducer installation

Figure 5. Heat flux transducer repositioned in the middle of the EPS

3.3 Material Properties Affecting the Thermal Response of Wall Systems

The thermal properties of the concrete layer of the ICF wall assembly are listed in Table 1 (Enermodal, 2006). Recently, the thermal conductivity and density of the type of EPS layer that was used in the ICF wall were measured at the NRC-IRC's material characterization laboratory at different temperatures. The test method used to measure the thermal conductivity of EPS was ASTM C 518-04 (2007). The measured thermal conductivity of EPS, λ_{eff} (in W/(mK)), as a function of temperature, T (in ^{o}C), that was used in the numerical simulation is given as:

$$\lambda_{eff} = 1.062 \times 10^{-4} T + 0.0308 \quad (1)$$

The uncertainty of the measured thermal conductivity of EPS was $\pm$1.5%. The measured density of EPS was 22.7 kg/m^3 (uncertainty = $\pm$0.6 kg/m^3).

There are four main parameters that affect the thermal response of a wall system. These parameters are:

1. Volumetric heat capacity, sometimes called thermal mass. This is a measure of the ability of the material to store thermal energy. In the case of the ICF wall, the concrete has the ability to store energy of 75 times that for EPS.
2. Thermal diffusivity, $\alpha = \lambda_{eff}/(\rho Cp)$. This is the ability of the material to conduct thermal energy relative to its ability to store thermal energy. The material with low thermal diffusivity responds slower to changes in the thermal environment compared to that with high thermal diffusivity. As shown in Table 1, the EPS respond to the thermal changes 3 times faster than the concrete.
3. Thermal resistance (R-value). It is a measure of the material ability to resist the heat flow. As shown in Table 1, both the ICF components have approximately an R-value of (R-20). By including the thermal resistance of the drywall in an ICF wall assembly, the total resistance can be 4.01 m^2K/W (R-22.8). Note that for the ICF wall, the thermal resistance of the concrete is much lower than the EPS. As such, the main contribution of the concrete in the ICF walls to thermal performance is to provide thermal mass and ability to store thermal energy.
4. Characteristic time constant, τ, is another parameter that affects the transient response of a wall system. It is defined as $\tau = L_p^2 / \alpha$, where L_p is the characteristic heat penetration length, which is equal to the thickness of material layer, δ. The characteristic time constant is a measure of the time that a material layer takes to complete 63.2% of the transient portion of its response due to a change in its thermal environment (63.2% response corresponds to 38.2% deviation from a steady-state condition, Rabin and Rittel, 1999). As shown in Table 1, the characteristic time constant of a 6" thick concrete (9.53 hr) is much larger than that for the 2.5" thick EPS (0.93 hr). As such, the exterior and interior EPS layers respond quickly to the changes in the indoor and outdoor conditions. On the other hand, the concrete layer responds slowly to changes of thermal environment resulting in a small change in its temperature as will be shown later.

Table 1. Dimension and thermal properties of the ICF components and glass fibre

Properties	**Concrete**	**EPS***
Thickness, δ, mm (inch)	152.4 (6")	63.5 (2.5")
Thermal Conductivity, λ_{eff} (W/(m.K))	1.4	0.0332
Density, ρ (kg/m^3)	2,350	22.7
Specific Heat, Cp (J/(kg.K))	880	1,210 (ASHRAE)
Volumetric Heat Capacity, ρCp ($kJ/(m^3.K)$)	2,068	27.47
Thermal Diffusivity, $\alpha = \lambda_{eff}/(\rho Cp)$ (m^2/s)	6.77×10^{-7}	1.21×10^{-6}
Characteristic Time Constant, $\tau = \delta^2/\alpha$ (hr)	9.53	0.93
Thermal Resistance, RSI = δ/λ_{eff} ($m^2.K/W$)	0.109	1.913
Total Thermal Resistance, R (ft^2 hr ^oF/BTU)	**22.3#**	

* Properties at 23°C

\# Value does not include the effect of thermal bridging due to the plastic spanners

4 Results

4.1 Outdoor Air Temperature

Outdoor air temperature data for the full field trial period is presented in Figure 6. This data is from the Ottawa International Airport (Environment Canada, 2010), located approximately 15 km South of the field trial location. The test period featured 3766 heating degree days below 18°C, and 322 cooling degree days above 18°C. The maximum temperature was 34.5°C and occurred July 8th 2010. The minimum temperature was -23.0°C, attained on January 30th 2010. The average, maximum and minimum monthly temperatures are given in Table 2.

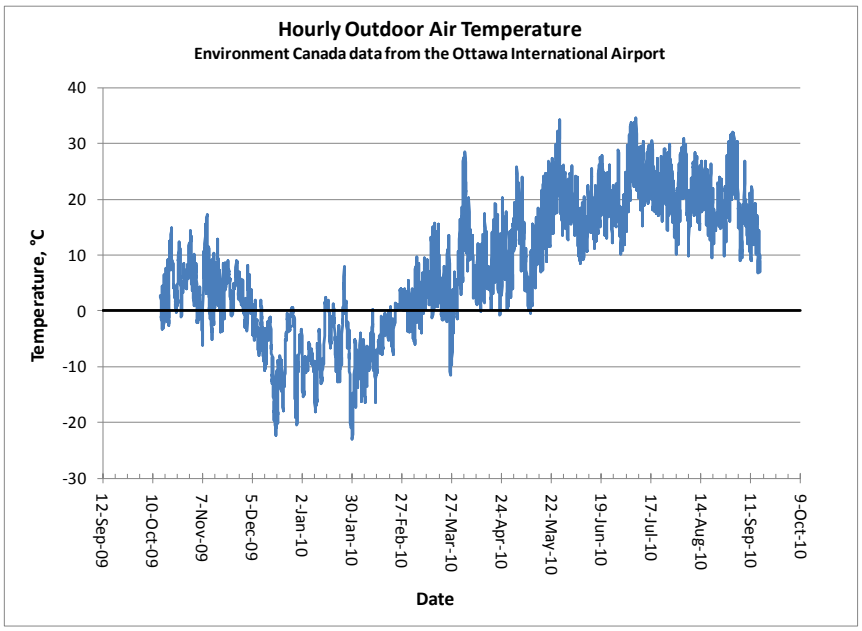

Figure 6. Outdoor Air Temperature, from the Ottawa International Airport (Environment Canada, 2010)

Table 2. Average, Maximum and Minimum Monthly Outdoor Air Temperature

Date	Average Outdoor T (°C)	Max Outdoor T (°C)	Min Outdoor T (°C)
13-Oct-09 to 31-Oct-09	5.3	14.9	-3.3
Nov-09	4.1	17.3	-6.1
Dec-09	-6.1	8.1	-22.3
Jan-10	-7.3	8.0	-23.0
Feb-10	-5.2	4.0	-17.2
Mar-10	3.1	16.4	-11.5
Apr-10	9.6	28.5	-0.7
May-10	15.8	34.2	-0.5
Jun-10	17.8	28.8	8.5
Jul-10	22.7	34.5	10.2
Aug-10	20.2	32.0	9.5
01-Sep-10 to 16-Sep-10	16.6	31.9	6.8

4.2 Indoor Air Temperature

The temperature of the air on the interior side of the ICF wall specimens is controlled by an indoor chamber. In winter, the chamber temperature is maintained above a 21°C setpoint by a heater. When the temperature drops below the setpoint, the heater is turned on. However, there is no control to prevent the chamber from overheating due to solar gains to the surrounding room. This overheating occurs primarily in the spring.

In summer, the chamber was opened and the maximum air temperature was controlled by the house's central cooling system.

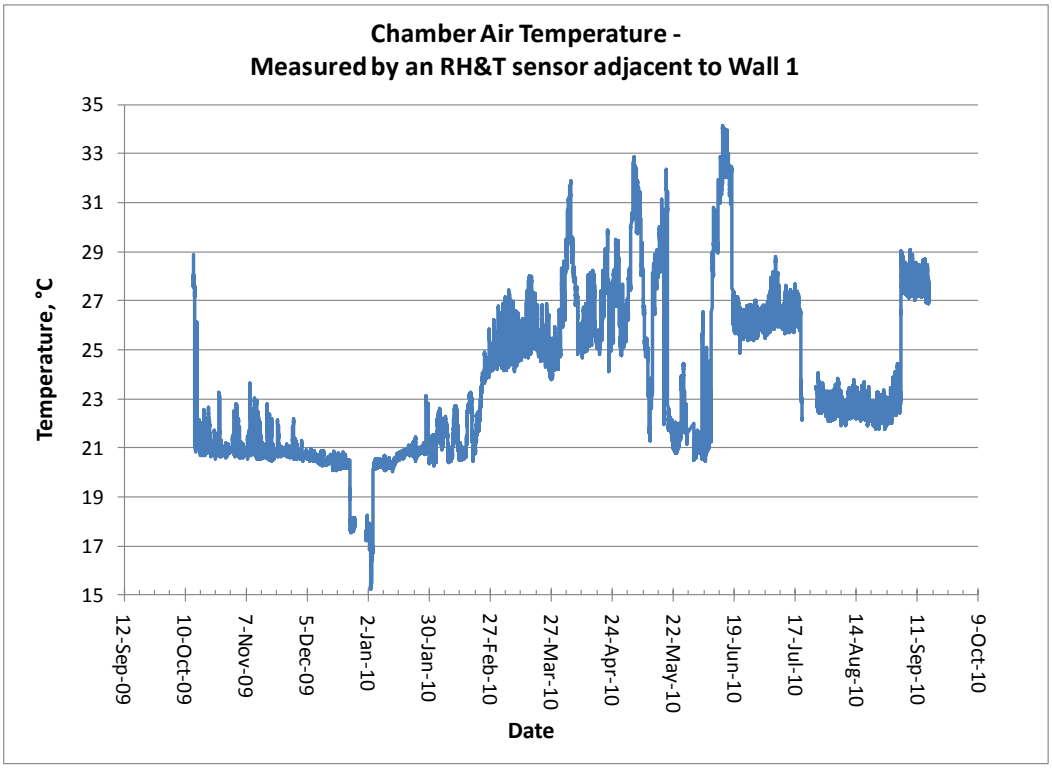

Figure 7. Chamber Air Temperature, as measured by an RH&T sensor adjacent to the interior surface of Wall 1

4.3 Surface Temperature

The average temperatures of the four different instrumentation layers are plotted in Figure 8: the exterior surface of the ICF (behind the siding), the exterior surface of the concrete, the interior surface of the concrete and the interior surface of the ICF (behind the drywall). The temperature measurements were taken every 15 minutes. The temperatures at the exterior and interior surface of the concrete are similar, due to the concrete's high conductivity. The largest difference between these two surface temperatures was 1.4°C, occurring on January 29th 2010. The temperatures at the surface of the concrete follow the general trends in outdoor temperature, reaching minimum temperatures in January. In summer, concrete surface temperatures are relatively steady – remaining around 20°C throughout the cooling season.

The interior surface temperature of the ICF (behind the drywall) is strongly influenced by the indoor air temperature – as controlled by the indoor chamber. In April and May, the interior surface temperature of the ICF was high, due to the overheating of the indoor air – as described in Section 4.2.

The temperature at the exterior of the ICF (behind the cladding) follows outdoor air temperature, and is also influenced by solar gains on the cladding in the afternoon/evening.

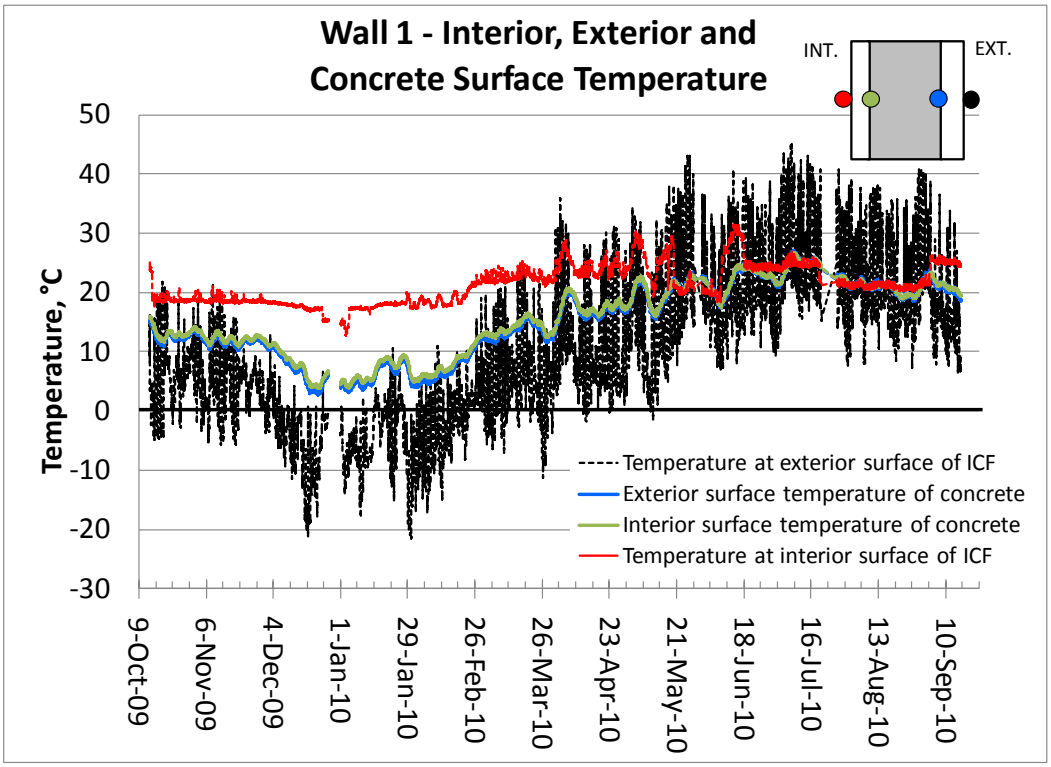

Figure 8. Measured 15-minute temperature data

4.3.1 Winter Surface Temperature

A detailed graph of the temperatures during February is provided in Figure 9. In addition to ICF and concrete surface temperatures, this graph also includes outdoor and chamber air temperatures. The exterior surface temperature of the ICF (behind the cladding) fluctuates daily with changes in outdoor temperature, and also heats up on sunny days up to 10°C above outdoor air temperature. The concrete provides a buffering effect – and its surface temperatures do not follow these up/down swings. The temperatures at both the interior and exterior surface of the concrete are relatively steady, increasing gradually from ~5°C to ~12°C with the general trend of increasing outdoor temperature. During this period, the indoor temperature was controlled in the chamber by the heater, and overheating did not occur. The temperature on the interior surface of the ICF (behind the drywall) was approximately 3°C cooler than the chamber air temperature. It looks like night radiations lowers the surface temperature below ambient conditions.

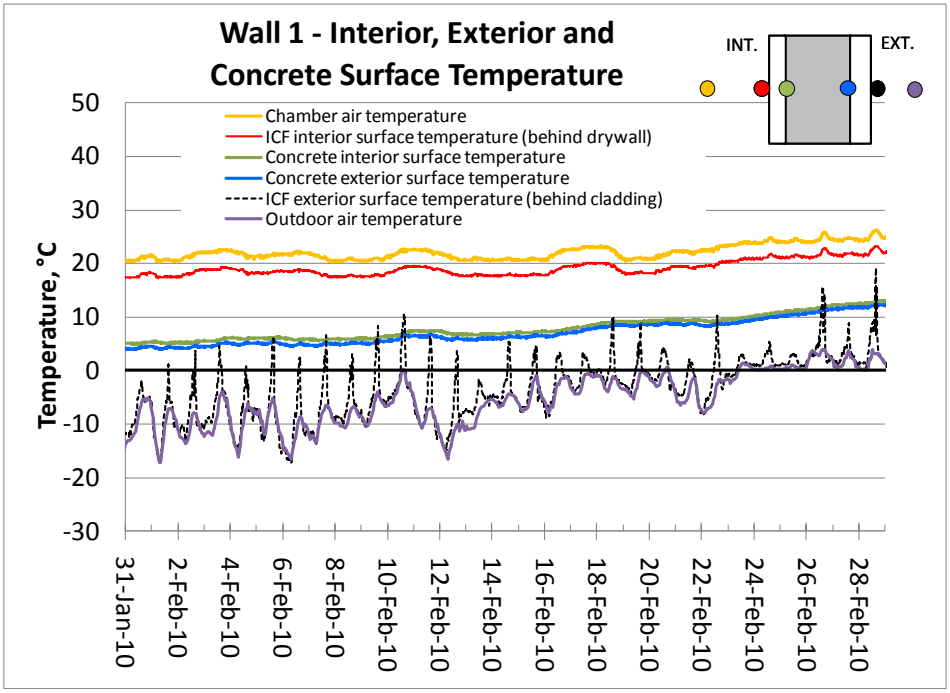

Figure 9. Winter detail of measured 15-minute temperature data

4.3.2 Summer Surface Temperature

Detailed 15-minute temperature measurements from August are shown in Figure 10. Throughout this month, the concrete surface temperatures are similar to the interior surface temperature of the ICF (plotted in red). All three surface temperatures (interior surface of the ICF, and interior and exterior surface of the concrete) are slightly (~1.5°C) cooler than the indoor chamber air temperature. The exterior temperature (plotted in black) fluctuates based on outdoor temperature, and is heated above the air temperature by solar radiation on sunny afternoons/evenings.

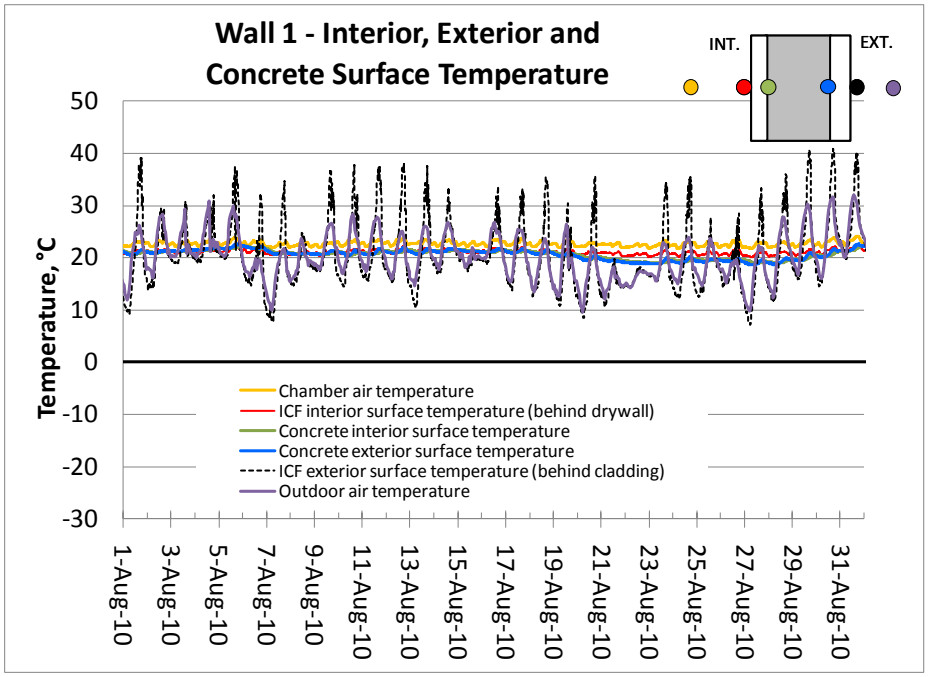

Figure 10. Summer detail of measured 15-minute temperature data

4.3.3 Relationship between Concrete Exterior Surface Temperature and ICF Exterior Surface Temperature

There is an apparent relationship between concrete exterior surface temperature and the general trend in exterior temperatures. To explore this further, the average daily concrete exterior surface temperature is plotted against the average daily exterior ICF surface temperature in Figure 11. The resulting relationship is linear with an R-square value of 0.9052.

Subsequently, the average temperature was plotted against a moving average of the exterior temperature of the ICF for the previously 2 days, 3 days, 4 days, etc. until the relationship with the strongest correlation was identified (with the highest R-squared value). The strongest relationship, with R-squared value of 0.971 was identified for the 5-day average (Figure 12). Thereby, the exterior concrete surface temperature has strong dependence on the ICF exterior temperature history from the previous 5 days. This gives an indication of the extent of the buffering effect of the ICF mass, even on the exterior side of the mass.

The average daily temperature at the exterior surface of the concrete is plotted alongside the moving 5-day average of the exterior surface temperature of the ICF in Figure 13. As expected from the high correlation factor (Figure 12), the two trends have a similar shape.

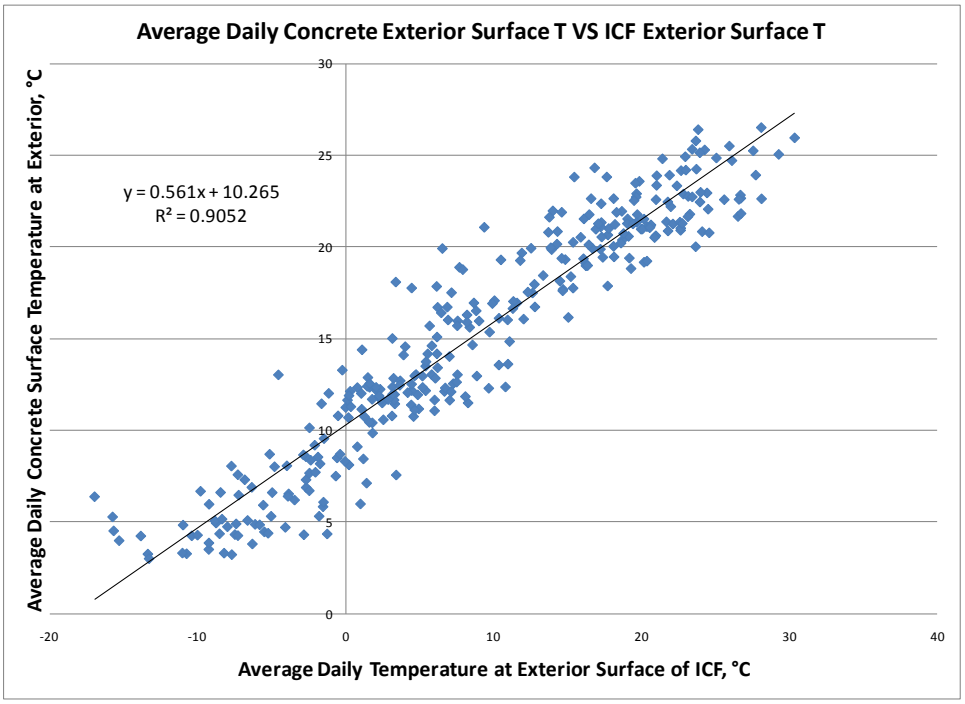

Figure 11. Average daily concrete exterior surface temperature vs. average daily ICF exterior surface temperature

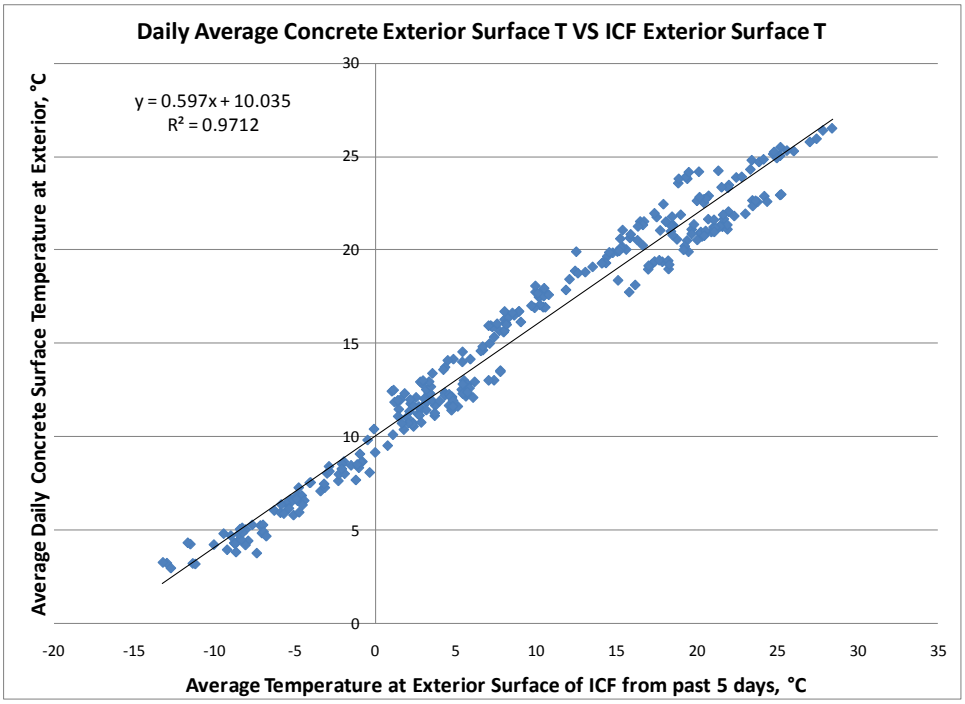

Figure 12. Average daily concrete exterior surface temperature vs. 5-day moving average of ICF exterior surface temperature

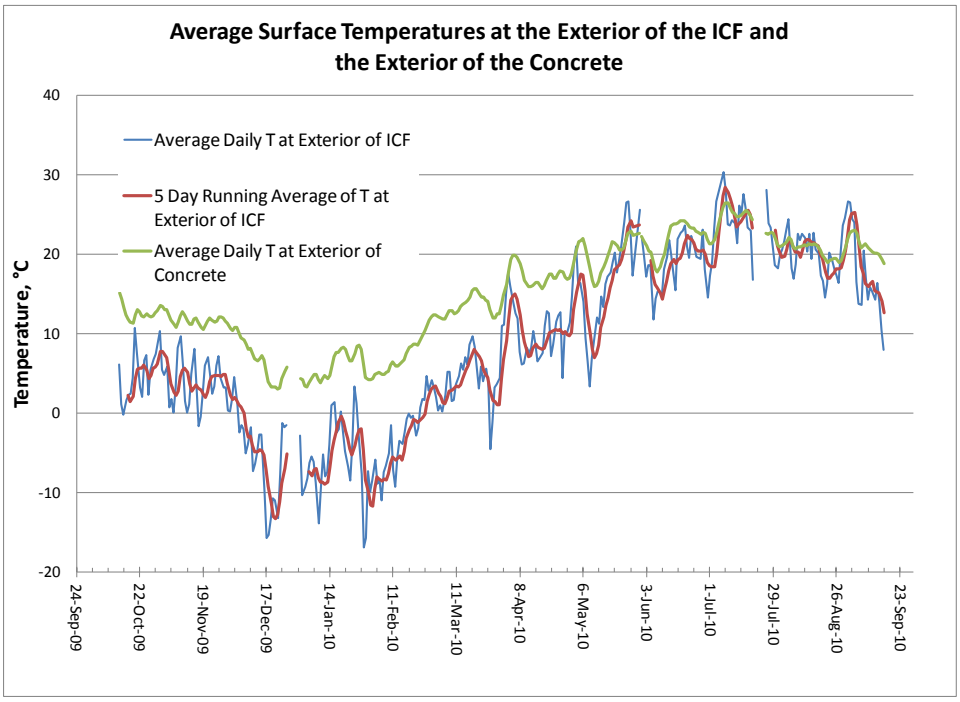

Figure 13. Average daily concrete exterior surface temperature and 5-day moving average of ICF exterior surface temperature

4.4 Heat Flux

The measured heat flux data (15-minute resolution) is presented in Figure 14. Heat flux flowing from the interior to the exterior side of the wall is considered positive. The higher the heat flux, the larger the heat loss from the interior, and the greater the load on the heating system.

Prior to January 14th for HF3 and January 29th for HF2, the positioning of the heat flux transducers resulted in erroneous readings (as described in Section 3.2). For this reason, measured heat flux data from the first few months of the experiment could not be used in this analysis. Heat flux from these months had to be calculated using the following method.

——— **(1)**

Where: T_{in}: interior temperature in °C
T_{ext}: exterior temperature in °C
q: heat flux in W/m^2

First, the average R-value of the foam either side of the concrete was calculated using the measured heat flux data (from the period following the repositioning of the heat flux sensors) and the delta T across the foam insulation, using Equation 1. The resulting R-values were: RSI 1.73, σ=0.09 (R 9.81, σ=0.52) for the interior foam, and 1.79 σ=4.32 (R 10.2 σ=24.5) for the exterior foam. The R-value for interior foam is in close agreement with the expected R-value of RSI 1.716 (R 9.74) based on ASHRAE's published value of thermal conductivity, 0.037 W/mK, (ASHRAE, 2009) and the thickness of the EPS, 64 mm (2.5 in.). The R-value of the exterior foam has a very high standard deviation due to large fluctuation in heat flux, and periodic low delta T across the exterior foam leading to reduced accuracy. Since both foams are identical, RSI 1.73 (R9.81) was assumed for both the exterior and interior insulation. This R-value was then combined with measured delta T across the interior and exterior insulation to predict the heat flux at location 2 and 3 for the first half of the experiment. This is referred to as "calculated" heat flux in Figure 14.

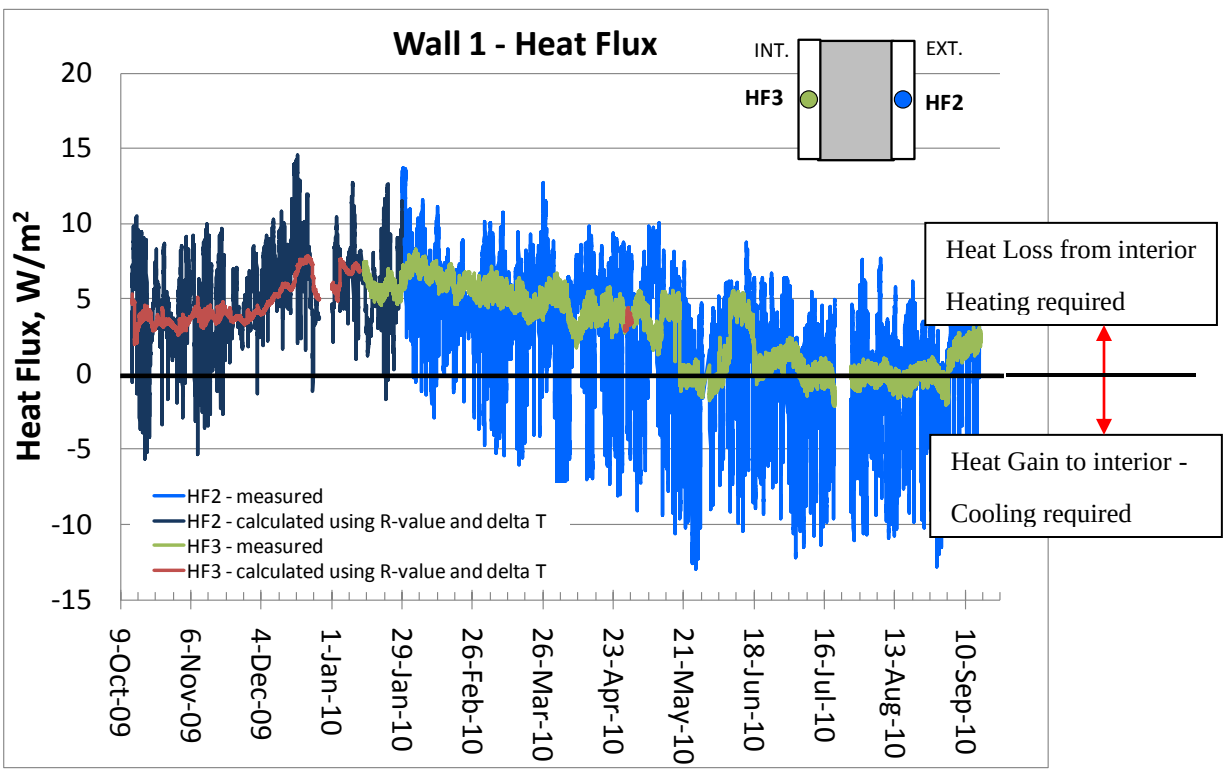

Figure 14. Heat flux at the interior and the exterior of the ICF (15-minute data)

The heat flux at the exterior of the ICF followed daily temperature swings caused by outdoor air temperature and solar effects in the afternoon, and ranged from 14.5 W/m^2 to -13.0 W/m^2. By contrast, the heat flux from the interior side of the ICF did not respond to the daily fluctuations in temperature, but rather followed the general temperature trend. The concrete mass evidently provided a buffering effect. As a result, the heat flux from the interior ranged from -2.2 W/m^2 to 8.3 W/m^2, primarily flowing from interior to exterior during the experiment period.

A detail of measured heat flux at the interior and exterior of the ICF during February is shown in Figure 15. The heat flux at the exterior of the concrete (HF2, plotted in blue) varies with outdoor conditions. When conditions outside are cold, heat flux is high, and when conditions outside are warm, heat flux is low. By contrast, heat flux leaving the room (HF3, plotted in green) is fairly constant since the concrete maintains a relatively steady trend in temperature, as seen in Figure 9. The heat flux leaving the room through the ICF wall is not immediately affected by cold nights outside, but also does not get the immediate benefit of reduced heat losses on warm days (Figure 15).

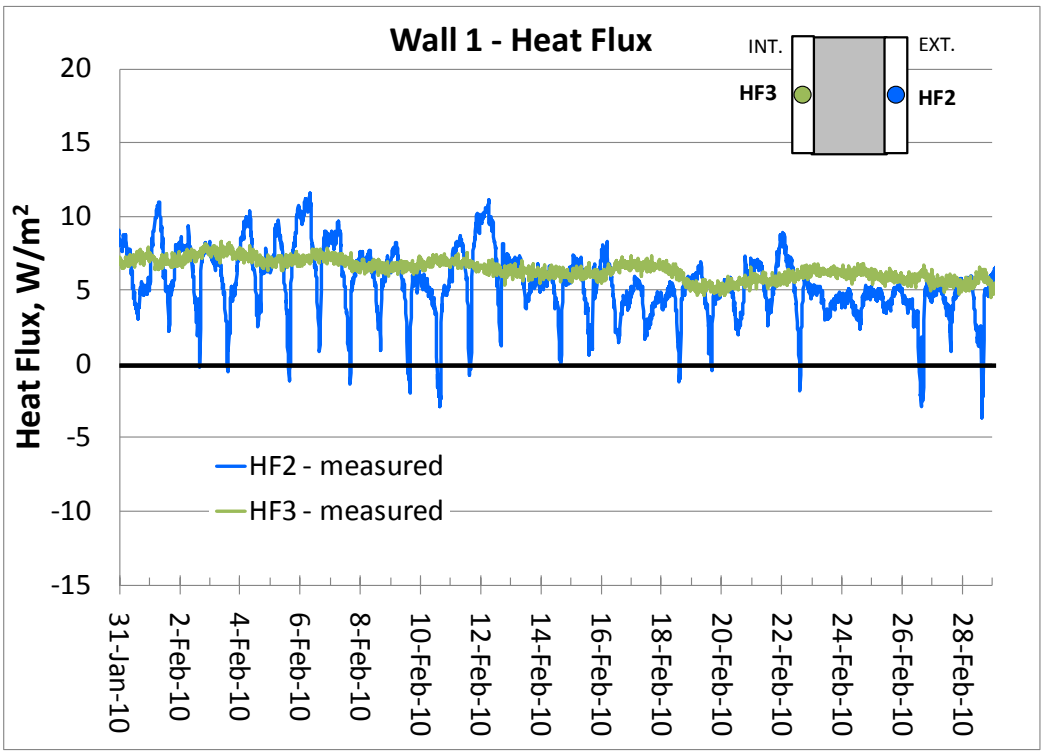

Figure 15. Detail of winter heat flux at the interior and the exterior of the ICF (15-minute data)

A detail of summer heat flux is given in Figure 16. The more negative the heat flux at HF3, the higher the heat gains to the interior of the home, and the higher the load on the cooling system. Because the temperature of the concrete is very close to the temperature of the interior throughout this period (Figure 10), there is almost no heat loss or gain at the interior (see HF3, plotted in green). The heat flux measured at the exterior foam (HF2, plotted in blue) by contrast cycles up and down. This is similar to the effects that would be seen in a wall with light weight construction and little mass effect (for more details see Section 4.7).

Since the ICF wall has very little heat flux from the interior during this time period, it would not experience a significant contribution to the peaks in cooling load from the ICF wall, as would be expected without the mass effect. However, the room does not immediately experience the benefit from free cooling overnight: rather, the free cooling is absorbed by the mass and presumably this helps to temper the effects of high outer surface temperature swings during the day, at times when peak air-conditioning would normally be experienced, both by the house and by the electric utility.

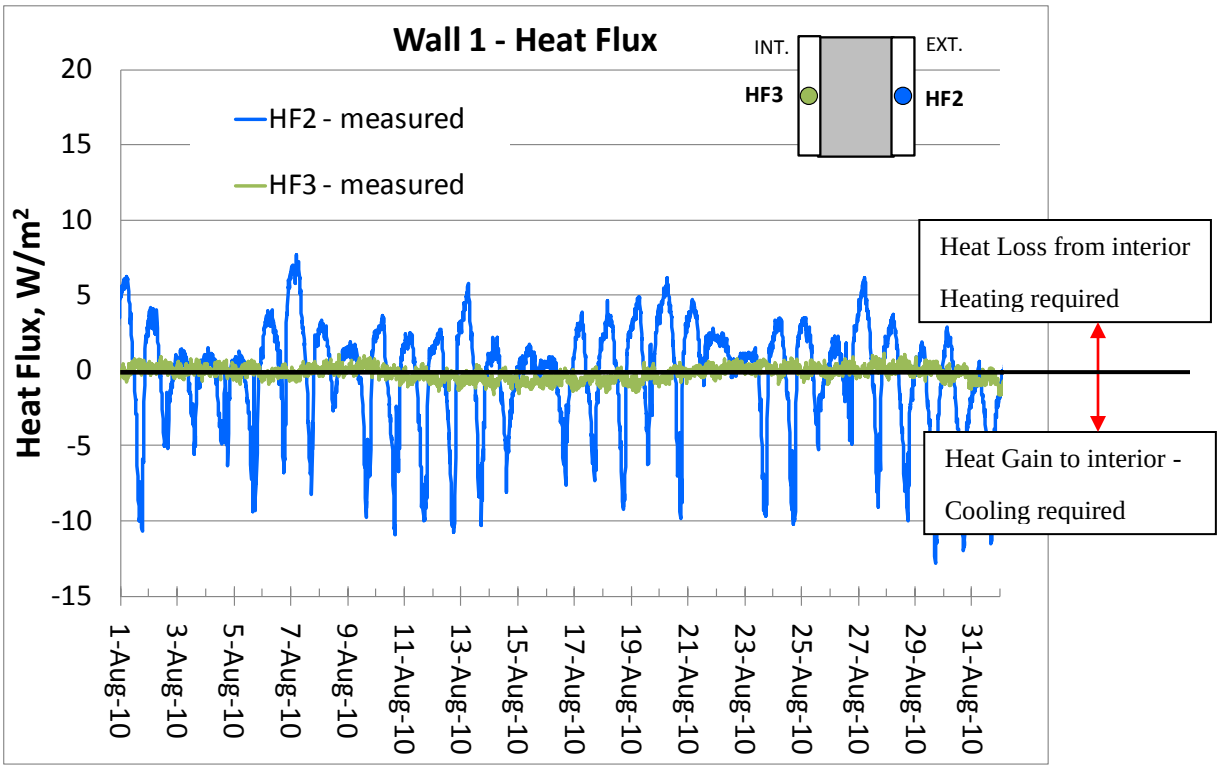

Figure 16. Detail of summer heat flux at the interior and the exterior of the ICF (15-minute data)

4.5 Pseudo Steady State R-value

On occasions where the heat flux on the exterior and the heat flux on the interior of the ICF are equal, the mass in the wall is neither storing nor releasing heat at that particular instant in time because its average temperature is temporarily constant (for example at the top or bottom of a temperature swing). During this condition, the wall is considered to be in a temporary or 'pseudo' steady state condition, where all of the heat transferred during that small time period is due to R-value only (see example in Figure 17). Using the measured data (delta T across the assembly and the heat fluxes) and Equation 1, the pseudo steady state R-value was calculated for all occasions where the absolute difference in measured heat fluxes (HF3-HF2) was less than 0.3 W/m^2. The result for Wall 1 is plotted in Figure 18. The average steady state RSI is 3.77 m^2 $^\circ C/W$, $\sigma = 0.15$ (R 21.4, $\sigma = 0.84$).

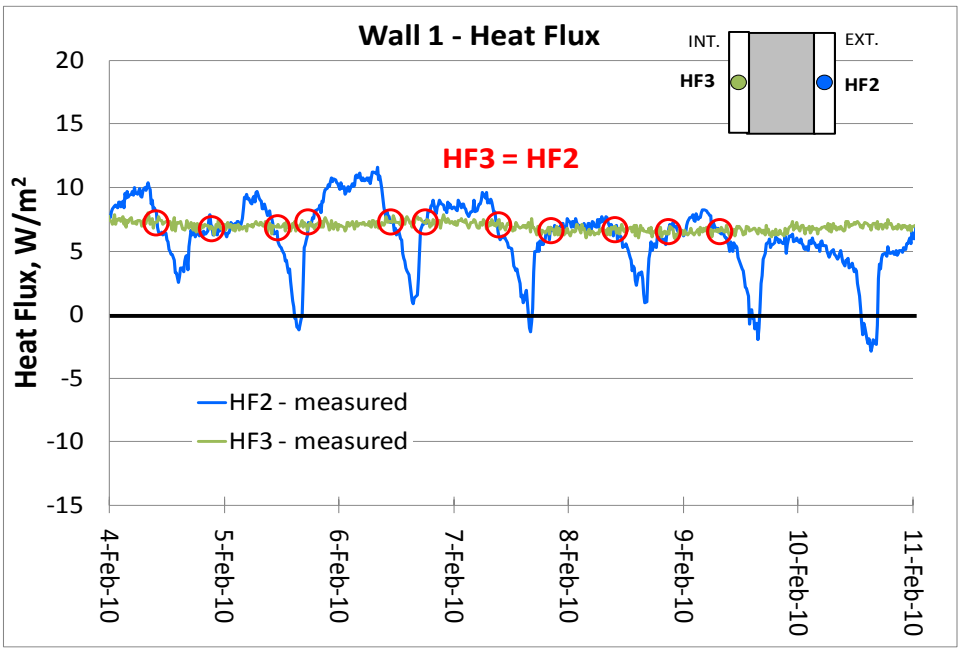

Figure 17. Example of occasions where the ICF wall is in "Pseudo Steady State"

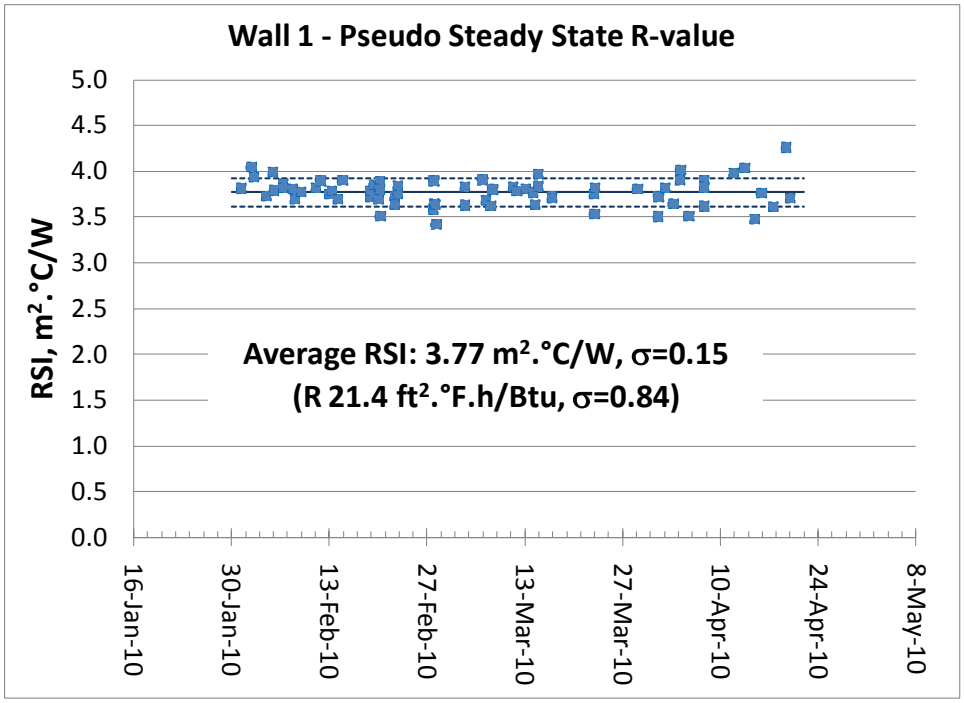

Figure 18. Pseudo Steady state R-value for the ICF

4.6 Heat absorbed and released by the concrete

Using the measured data, the heat absorbed and released by the concrete during each 15 minute timestep can be determined in two ways: using the difference in measured heat flux (Equation 2), and using the change in the average temperature of the concrete (Equation 3) – obtained by averaging the temperatures at the exterior and interior surface of the concrete (layers 2 and 3).

(2)

Where: Q: total heat, Wh
q_{in}: heat flux at the interior, W/m^2
q_{ext}: heat flux at the exterior, W/m^2
A: interior surface area of concrete, 2.76 m^2
t: timestep, 0.25 h

(3)

Where: Q: total heat, Wh
ρ : density of concrete, 2350 kg/m^3
V: volume of concrete, 0.42 m^3
C_p: specific heat capacity of concrete, 0.244 Wh/kg°C (880 J/kgK)
T_i: Average temperature of concrete at current time, °C
T_{i-1}: Average temperature of concrete at previous time, °C

The total daily heat absorbed (+ve) or released (-ve) by the concrete in the ICF is plotted in Figure 19. Both methods of calculating the heat absorbed and released give an approximately similar result. Small differences are present, and may be due to the assumed properties for the concrete (Cp=880 J/kgK, ρ=2350 kg/m^3), or the accuracy of the heat flux transducers. The similarity of the two trends gives confidence in the heat flux transducer readings.

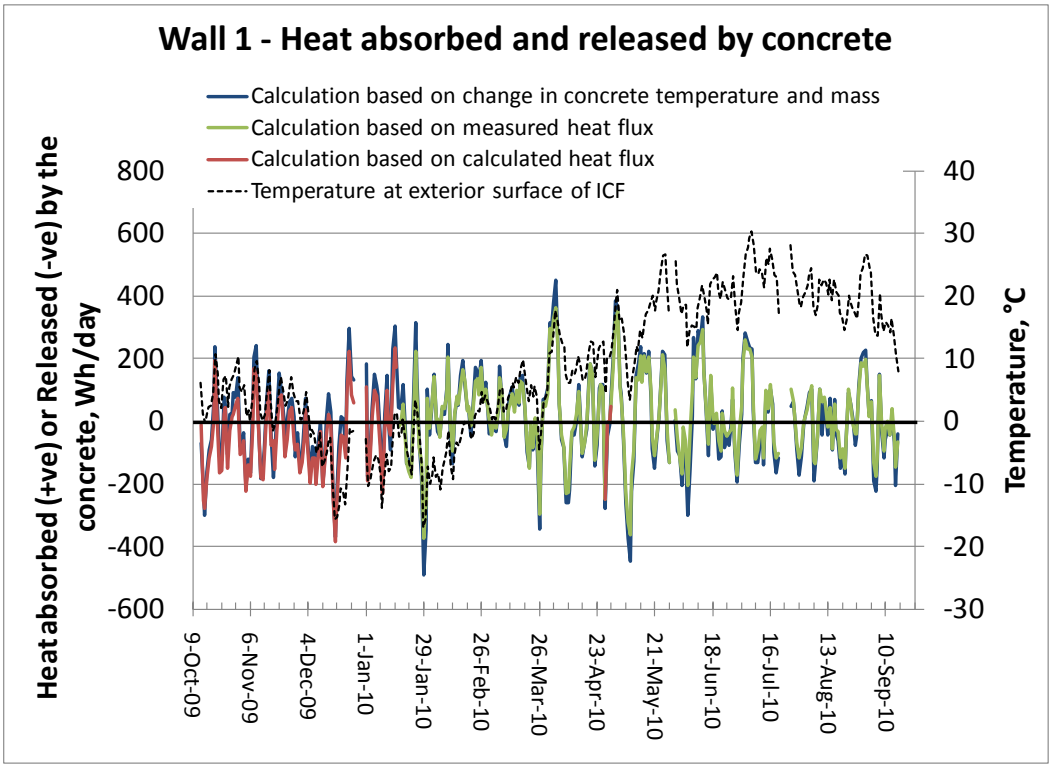

Figure 19. Daily heat absorbed and released by the concrete

4.7 Impact of mass on heat flux

The heat flux at the interior of the ICF, leaving the interior of the home, is of greatest interest since it has an impact on heating and cooling system requirements and also a potential impact on the sizing mechanical equipment. For this reason, the performance of the ICF was compared with the theoretical performance of the same wall without mass effect. Heat flux without mass (due to conduction alone), was determined using Equation 1, the steady state R-value (RSI 3.77 ±4% [R 21.4 ±4%]) and the measured average temperatures at the exterior and interior surface of the ICF throughout the experiment. While the wall itself may have some small impact on these measured temperatures, this impact was assumed to be small, and verified to be small in a subsequent study.

The resulting comparison of the wall with and without mass is shown in Figure 20. Without thermal mass, the heat flux varies significantly with change in outdoor temperature, following daily swings. With the effect of thermal mass, however, the heat flux varies only slightly during each day.

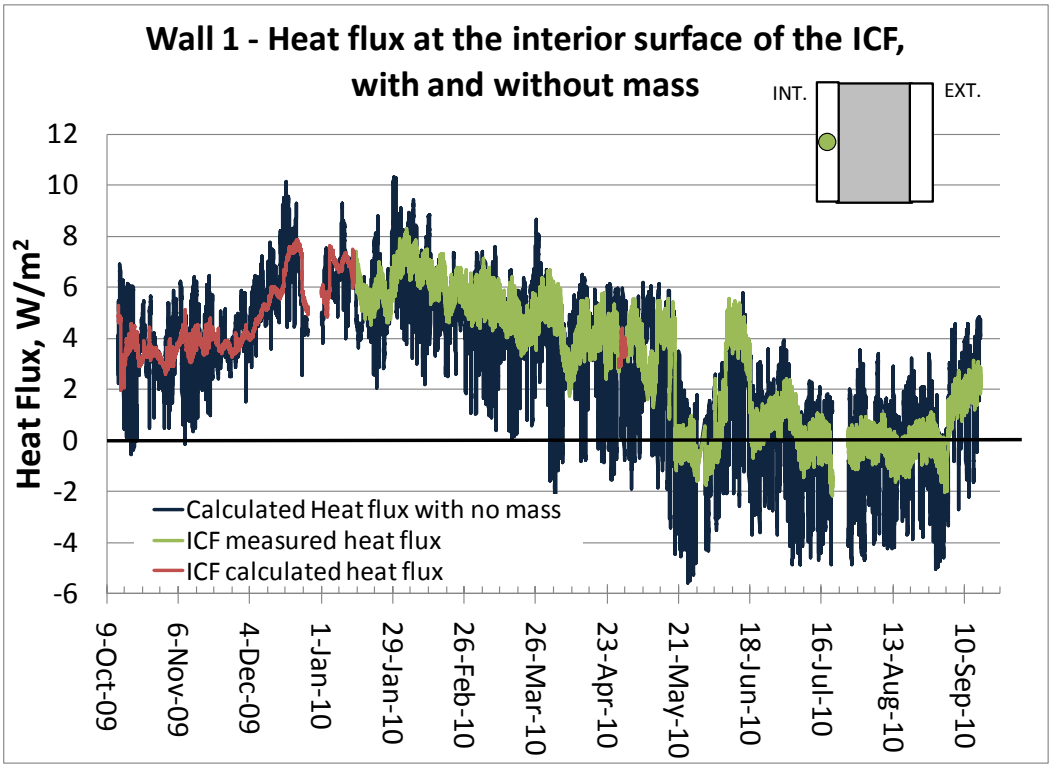

Figure 20. Heat flux at the interior surface of the ICF, with and without mass (15-minute timestep)

Details of this mass/no mass comparison for February and August are provided in Figure 21 and Figure 22 respectively. In February, heat flux on the interior side of the ICF wall is fairly steady. Whereas, predicted heat flux at this same location in a wall with no mass fluctuates on a daily basis with changes in outdoor temperature. In August, the measured heat flux at the interior of the ICF is close to zero. During this same period, the calculated heat flux for the wall with no mass cycles daily above and below zero: at night heat is lost from the room (+ve heat flux), and during the day heat is gained by the room (-ve heat flux). Heat gains in summer contribute to the cooling load of the air conditioning system i.e additional cooling is required in the room to maintain constant temperature.

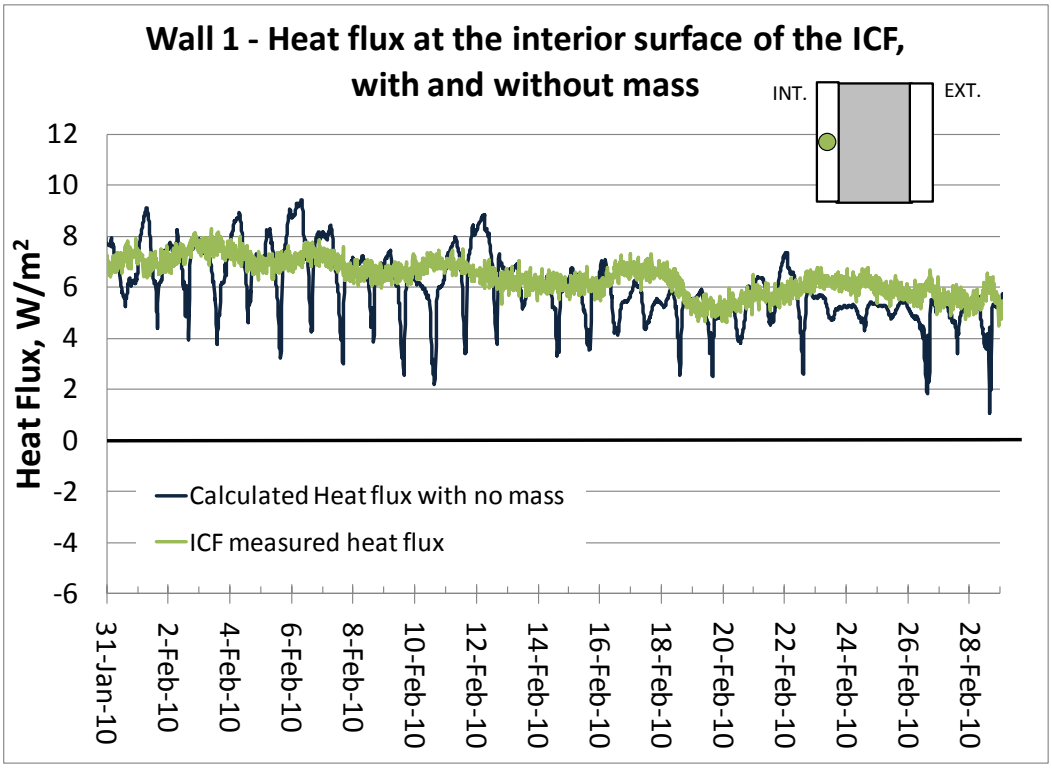

Figure 21. February detail of heat flux at the interior surface of the ICF, with and without mass (15-minute timestep)

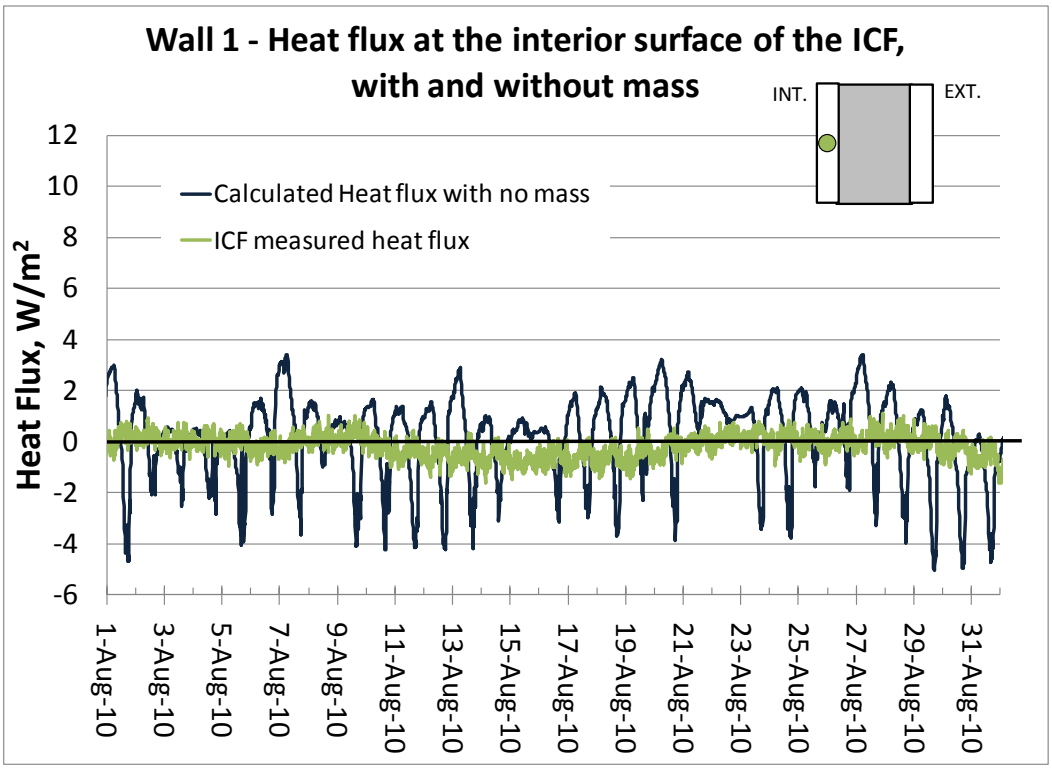

Figure 22. February detail of heat flux at the interior surface of the ICF, with and without mass (15-minute timestep)

4.7.1 Monthly heat loss and gain

The total monthly heat loss, heat gain and net heat loss (loss minus gain) from the room to the wall are listed in Table 3. This table includes the measured heat loss/gain for ICF Wall 1 and the calculated heat loss/gain for a wall with no mass and RSI 3.77 (R 21.4).

Despite the mass of the ICF wall providing a buffering effect against daily fluctuations in outdoor temperature (as shown in the previous section), there is only a small difference in the cumulative monthly heat loss between the measured ICF value and the expected value for a wall with no mass. This is illustrated in the bar chart in Figure 23, and the heating season cumulative graph in Figure 24. On a monthly basis there is evidence of the mass buffering effect: The ICF wall shows lower cumulative heat loss than the "no mass" wall from October to December, as the ICF stores heat as the general trend in outdoor temperature drops. From January through May, the opposite is true – wth the ICF wall having a higher cumulative heat loss, as it is slower to respond to warming outdoor temperatures than the "no mass" wall. Over the full heating season (Figure 24), there was only a 1% difference in cumulative heat loss. This difference falls within the accuracy of heat flux sensor readings.

In summer, the cumulative monthly heat gain to the interior of both walls is relatively small – compared to the winter heat losses (see Figure 25). However, the percentage differences in heat gain between the ICF wall and the "no mass" wall are larger. Over the cooling season, thanks to the mass buffering effect, the ICF wall had a 60.8% lower cumulative heat gain than the wall with "no mass" (Figure 26).

Table 3. Comparison of the Total Monthly Heat Gain and Losses at the interior of an ICF and an RSI 3.77 (R 21.4) wall with no mass.

	ICF (HFT 3)			Wall with no mass* RSI 3.77 (R 21.4)			Difference due to mass		
Date	Measured Heat Loss from Interior, kWh/m^2	Measured Heat Gain to Interior, kWh/m^2	Net Measured Heat Loss, kWh/m^2	Calculated Heat Loss from Interior, kWh/m^2	Calculated Heat Gain to Interior, kWh/m^2	Net Calculated Heat Loss, kWh/m^2	Heat Loss from Interior, kWh/m^2	Heat Gain to Interior, kWh/m^2	Net Heat Loss, kWh/m^2
13-Oct-09 to 31-Oct-09	1.53	0.00	1.53	1.63	0.00	1.62	-0.10	0.00	-0.09
Nov-09	2.70	0.00	2.70	2.84	0.00	2.84	-0.13	0.00	-0.13
01-Dec-09 to 26-Dec-09	3.55	0.00	3.55	3.75	0.00	3.75	-0.20	0.00	-0.20
Jan-10	4.61	0.00	4.61	4.55	0.00	4.55	0.06	0.00	0.06
Feb-10	4.29	0.00	4.29	4.02	0.00	4.02	0.27	0.00	0.27
Mar-10	3.79	0.00	3.79	3.67	0.00	3.66	0.13	0.00	0.13
Apr-10	2.89	0.00	2.89	2.73	0.02	2.71	0.16	-0.02	0.18
01-May-10 to 28-May-10 & 31-May-10	1.70	0.08	1.62	1.65	0.27	1.38	0.05	-0.18	0.23
Jun-10	1.27	0.06	1.21	1.26	0.19	1.07	0.01	-0.12	0.14
01-Jul-10 to 20-Jul-10, 26-Jul-10 to 31-Jul-10	0.23	0.14	0.09	0.45	0.43	0.01	-0.22	-0.30	0.07
Aug-10	0.08	0.20	-0.12	0.58	0.42	0.15	-0.50	-0.22	-0.28
01-Sep-10 to 16-Sep-10	0.55	0.07	0.49	0.83	0.08	0.75	-0.28	-0.01	-0.27

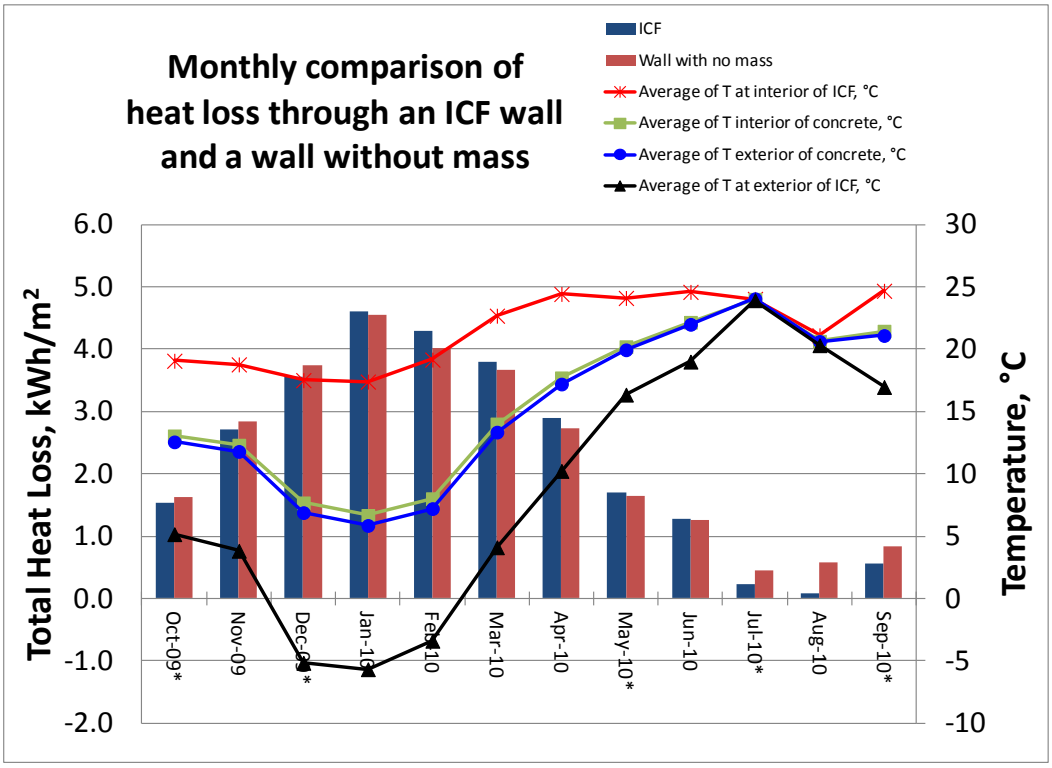

* incomplete months (see Table 3)

Figure 23- Monthly comparison of heat loss through an ICF wall and a wall with no mass.

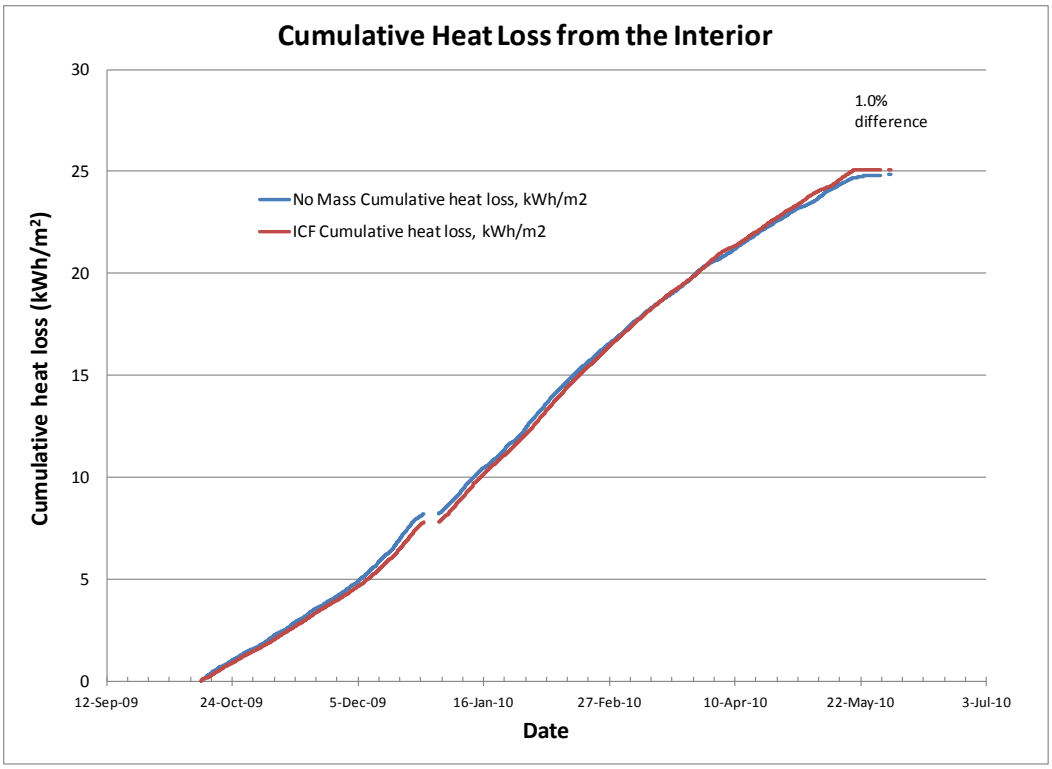

Figure 24- Cumulative energy loss for walls with and without mass (heating season only).

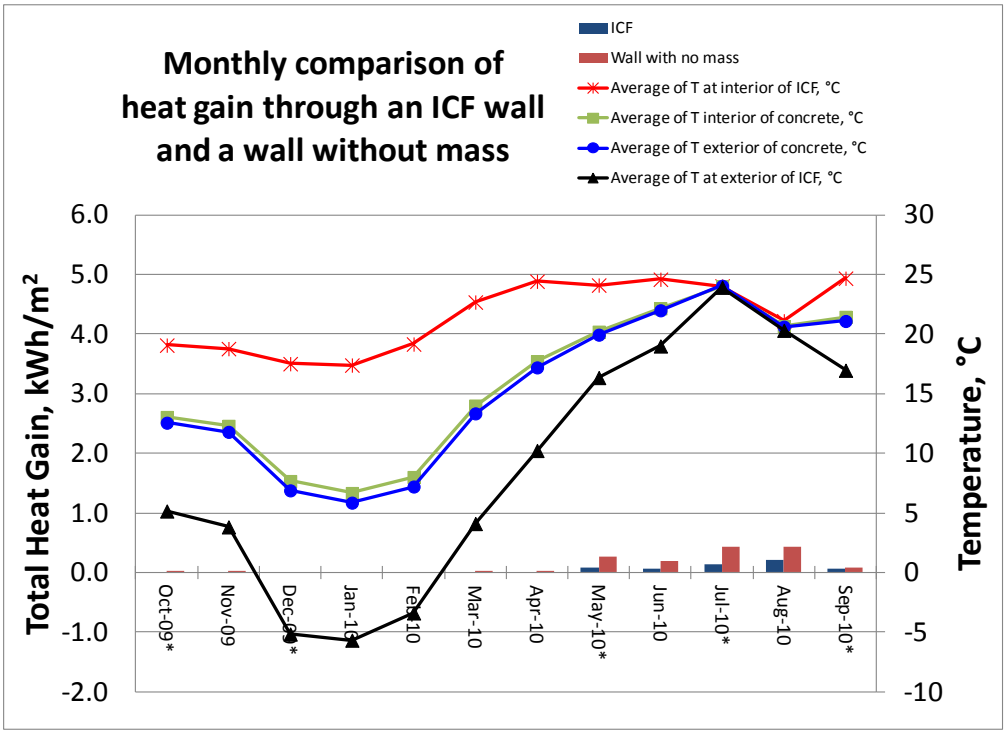

*Incomplete months (see Table 3 Comparison of the Total Monthly Heat Gain and Losses at the interior of an ICF and an RSI 3.77 (R 21.4) wall with no mass.)

Figure 25. Monthly comparison of heat gain through the ICF, and a wall without mass

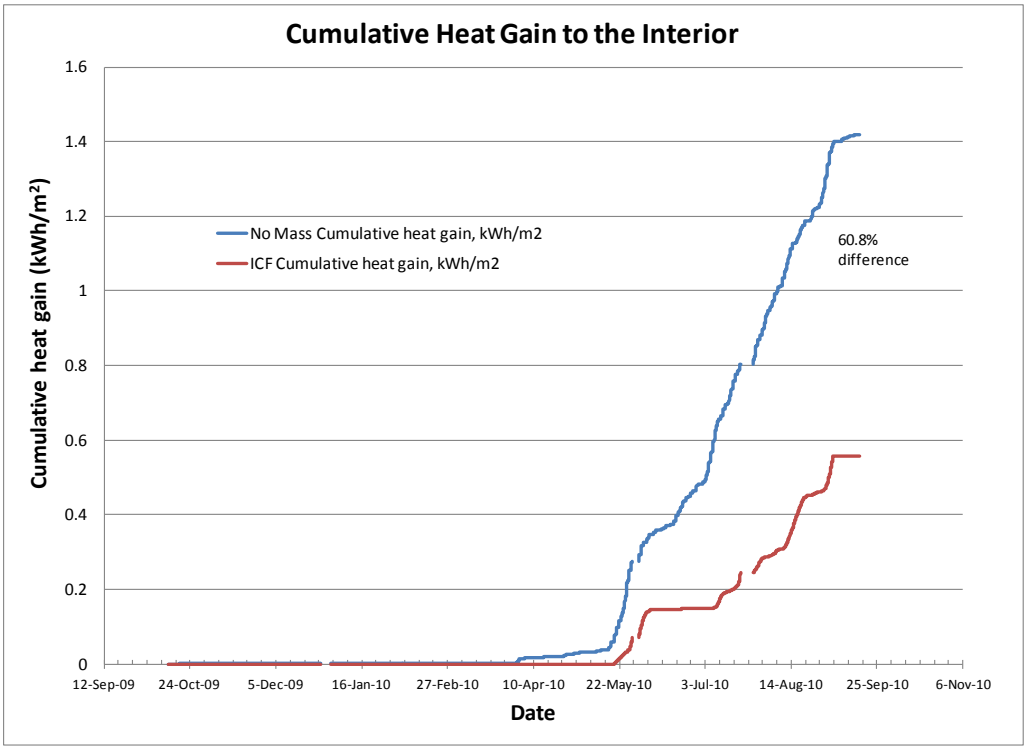

Figure 26 - Cumulative energy gain for walls with and without mass.

4.7.2 Monthly maximum and minimum heat flux

A monthly comparison of 15-minute measured heat flux at the interior side of the ICF, and predicted heat flux at this same location for a wall with no mass is given in Figure 27. Each point on this graph indicates the average monthly heat flux for either the ICF wall (blue) or the no mass wall (pink). The top and bottom of the bars associated with each point indicate the monthly maximum and minimum 15-minute heat flux values.

While the total monthly heat loss is similar for the two walls (see Section 4.7.1), the maximum and minimum values differ as a result of the buffering effect of the mass. The measured 15-minute peak in heat flux for the ICF was 8.3 W/m^2 (Feb-10), and the peak 15-minute heat flux without mass is predicted to be 10.3 W/m^2 (Jan-10). This 2.0 W/m^2 different in peak heat flux would likely have an impact on the heating load of a home, and the sizing of heating equipment.

In summer, the minimum heat flux for the ICF wall was -2.2 W/m^2. The expected minimum heat flux across the wall with no mass is -5.6 W/m^2, resulting in a 3.4 W/m^2 higher cooling load. Again, this could have implications for the sizing of an air conditioning system.

The monthly maximum and minimum 15-minute heat flux values are provided in Table 4.

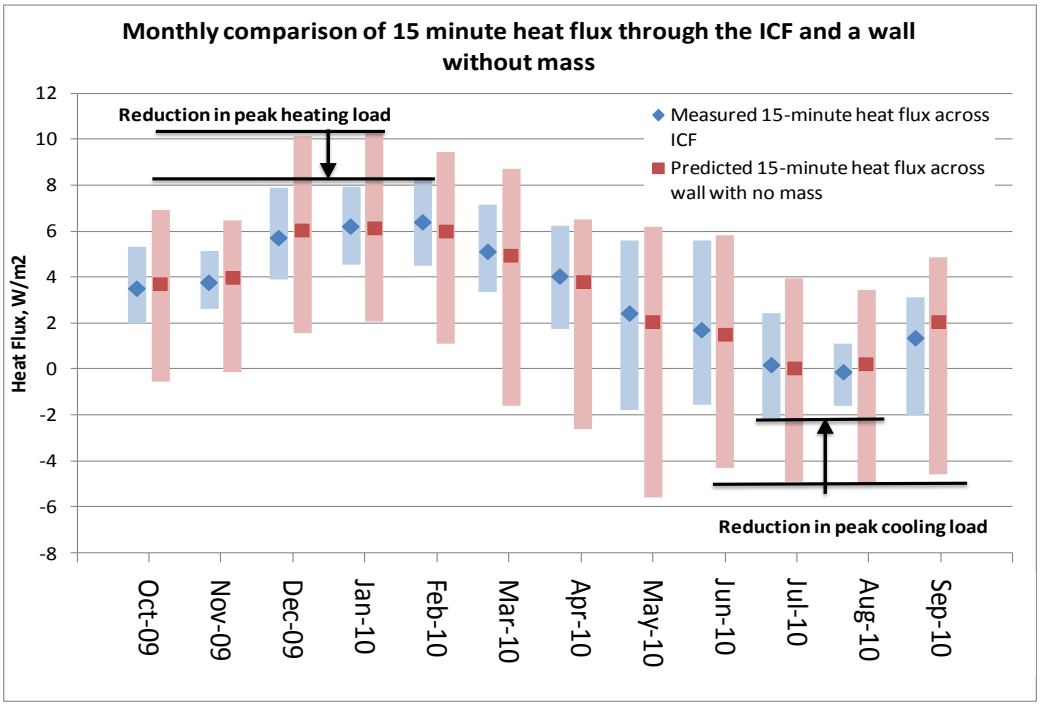

Figure 27. Monthly comparison of 15-minute heat flux through the ICF and a wall with no mass. (Each point represents the average monthly heat flux, with the bars indicating the monthly maximum and minimum heat flux values.)

Table 4. Comparison of the Maximum and Minimum Monthly Heat Flux at the interior of an ICF and an RSI 3.77 (R 21.4) wall with no mass.

	Maximum 15-minute Heat Flux			Minimum 15-minute Heat Flux		
	ICF Measured Heat Flux (HFT 3)	RSI 3.77 (R 21.4) Wall with no mass calculated heat flux	Difference	ICF Measured Heat Flux (HFT 3)	RSI 3.77 (R 21.4) Wall with no mass calculated heat flux	Difference
Date	W/m^2	W/m^2	W/m^2	W/m^2	W/m^2	W/m^2
13-Oct-09 to 31-Oct-09	5.3	6.9	-1.6	2.0	-0.6	2.6
Nov-09	5.1	6.4	-1.3	2.6	-0.1	2.7
01-Dec-09 to 26-Dec-09	7.9	10.1	-2.3	3.9	1.5	2.4
Jan-10	7.9	**10.3**	-2.4	4.5	2.1	2.5
Feb-10	**8.3**	9.4	-1.2	4.5	1.1	3.4
Mar-10	7.1	8.7	-1.6	3.3	-1.6	4.9
Apr-10	6.2	6.5	-0.3	1.8	-2.6	4.4
01-May-10 to 28-May-10 &31-May-10	5.6	6.2	-0.6	-1.8	**-5.6**	3.8
Jun-10	5.6	5.8	-0.2	-1.5	-4.3	2.8
01-Jul-10 to 20-Jul-10, 26-Jul-10 to 31-Jul-10	2.4	3.9	-1.5	**-2.2**	-4.9	2.7
Aug-10	1.1	3.4	-2.3	-1.6	-5.0	3.4
01-Sep-10 to 16-Sep-10	3.1	4.9	-1.7	-2.0	-4.6	2.6

5 Wall 1 compared to Wall 2

The analysis in this report centres on results from the first of the two wall specimens – ICF Wall 1. While data was collected from both walls, the ICF Wall 2 results were discarded from the analysis due to the reasons outlined in this section.

5.1 Difference in Interior Temperature

Even though Wall 1 and Wall 2 were exposed to the same naturally occurring outdoor conditions, and the same interior controlled chamber conditions, there were significant differences in measured temperatures. The average monthly surface temperatures of the two ICF walls are compared in Figure 27. The largest difference between the two walls is seen at the interior surface of the ICF. This difference is shown in greater detail inFigure 28. In this graph, the 15-minute average interior surface temperature is plotted for the two ICF wall specimens on the secondary y-axis (right axis), and the difference between the two curves is plotted in blue on the primary y-axis (left axis). Starting in February, The Wall 2 ICF interior surface temperature was warmer than the Wall 1 ICF interior surface temperature – typically between 0.5 and 1°C warmer. For a short period between mid-May and mid-June Wall 2 temperature was up to 3°C warmer than the Wall 1 ICF interior surface temperature.

The location of the heater in the interior chamber and its mode of operation is a likely explanation for the difference in interior ICF surface temperature. The heater in the chamber is a standard home space heater with internal fan. When the setpoint temperature in the chamber is satisfied (as measured by an RH&T sensors mounted centrally in the chamber), the power to the heater is shut off. As a result, both the heater's heating coil and the internal fan shut off. Natural operation of the heater would require the internal fan to run to dissipate heat for a short period of time after the heat coil was shut off. However, the control system simply shut off the power to both at once, thereby leaving the heating coil warm. The chamber heater is located near Wall 2. The heater is aimed away from the surface of Wall 2. However, when the heater turns off abruptly heat that would otherwise be circulated to the full chamber potentially has a larger impact on the surface of Wall 2 (in closer proximity) than the surface of Wall 1. This could potentially explain why differences in surface temperature between the two walls increased in warmer weather (in the spring), when the heater (and fan) would operate less frequently, and also why the temperature difference disappeared in August.

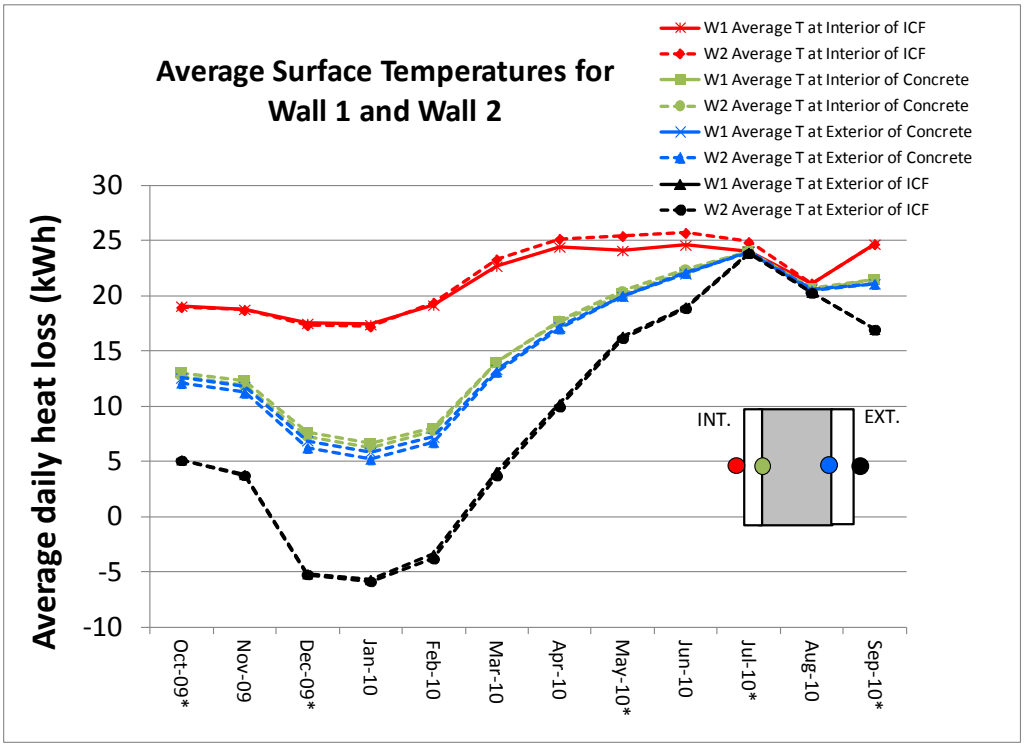

Figure 28. Comparison of Wall 1 and Wall 2 temperature measurements

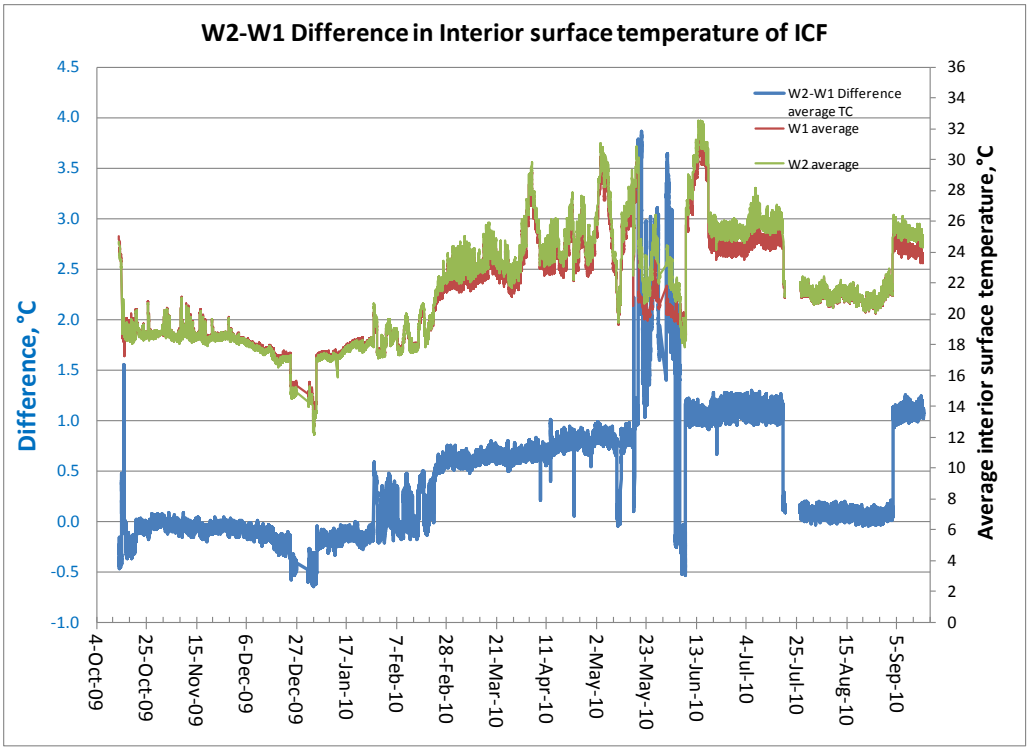

Figure 29. Difference in the ICF interior surface temperature for Wall 1 and Wall 2

5.2 Difference in Heat Flux

Measured 15-minute heat flux from Wall 1 and Wall 2 are compared in Figure 29. Each point on this graph indicates the average monthly heat flux for either the Wall 1 (blue) or Wall 2 (pink). The top and bottom of the bars associated with each point indicate the monthly maximum and minimum 15-minute heat flux values. The average, maximum and minimum measured monthly heat flux values for Wall 2 are generally lower than the measured monthly heat flux for Wall 1.

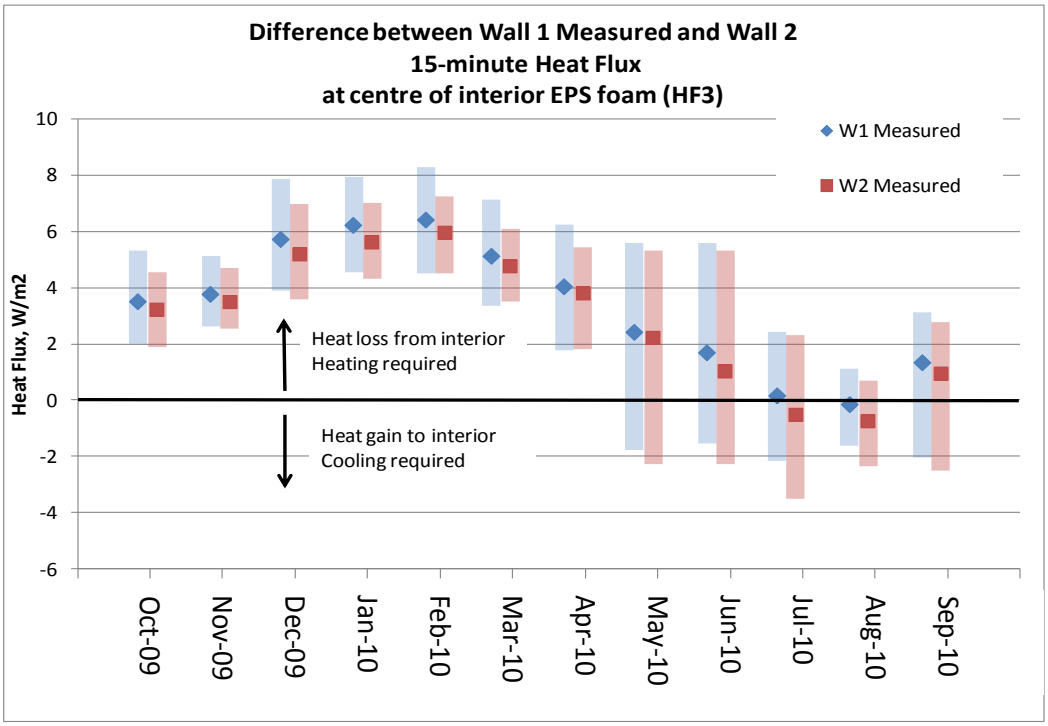

Figure 30. Comparison of Wall 1 and Wall 2 measured Heat Flux at the Centre of the Interior EPS Foam (HF3). Each point represents the average monthly heat flux, with the bars indicating the monthly maximum and minimum heat flux values.

In order to determine which heat flux values (Wall 1 or Wall 2) are most accurate, the values were compared to modeling results. For a full description of the model and comparison, refer to the ICF model report by Saber, 2011. The model-predicted heat flux is compared to the measured heat flux in Figure 30 and Figure 31 for Wall 1 and Wall 2 respectively. The initial conditions for the model were different than the conditions at the start of the experiment – thus the comparison can only be considered after the first two weeks. Wall 1 measured heat flux compares closely to the modeled heat flux for the full period. Wall 2 measured heat flux is also close to the model prediction for the first portion of the experiment, but differs from 17-May-10 onwards. On this date, the heat flux transducer at location HFT3 in Wall 2 was replaced, and unfortunately this resulted in erroneous data.

Due to the overheating of the interior of Wall 2, and the likely error in Wall 2 heat flux (HFT3) measurement after 17-May-10, Wall 1 data was chosen for the detailed analysis presented in this report.

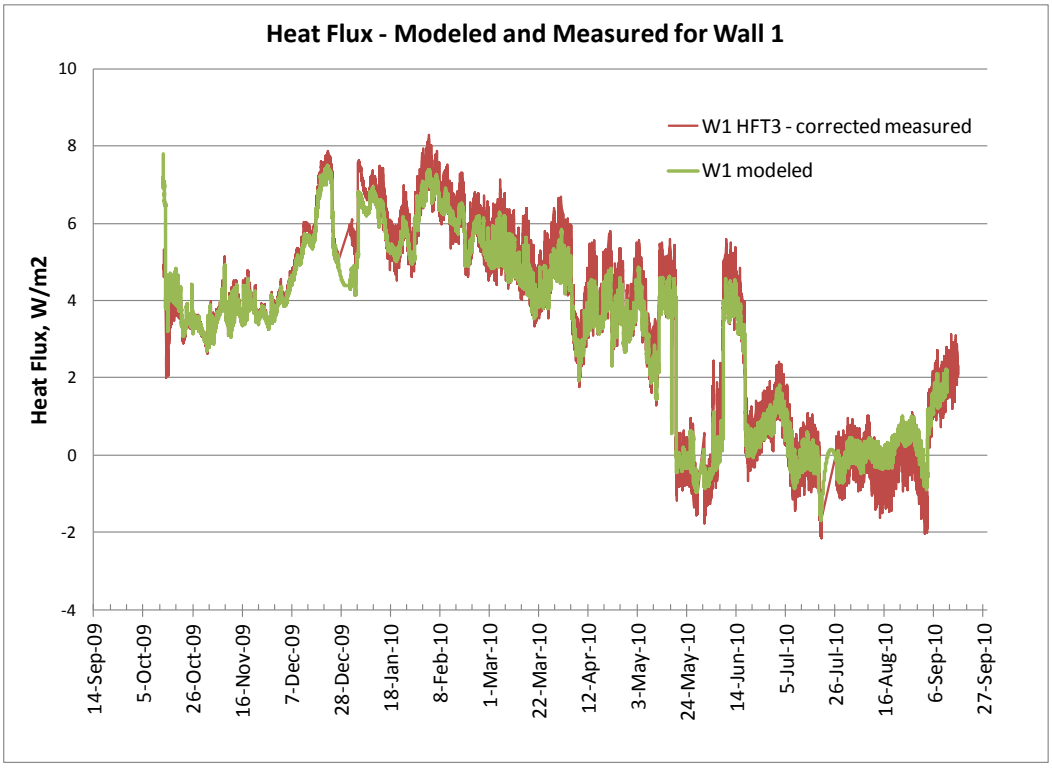

Figure 31. Comparison of the modeled heat flux and measured heat flux at location HFT3 for Wall 1.

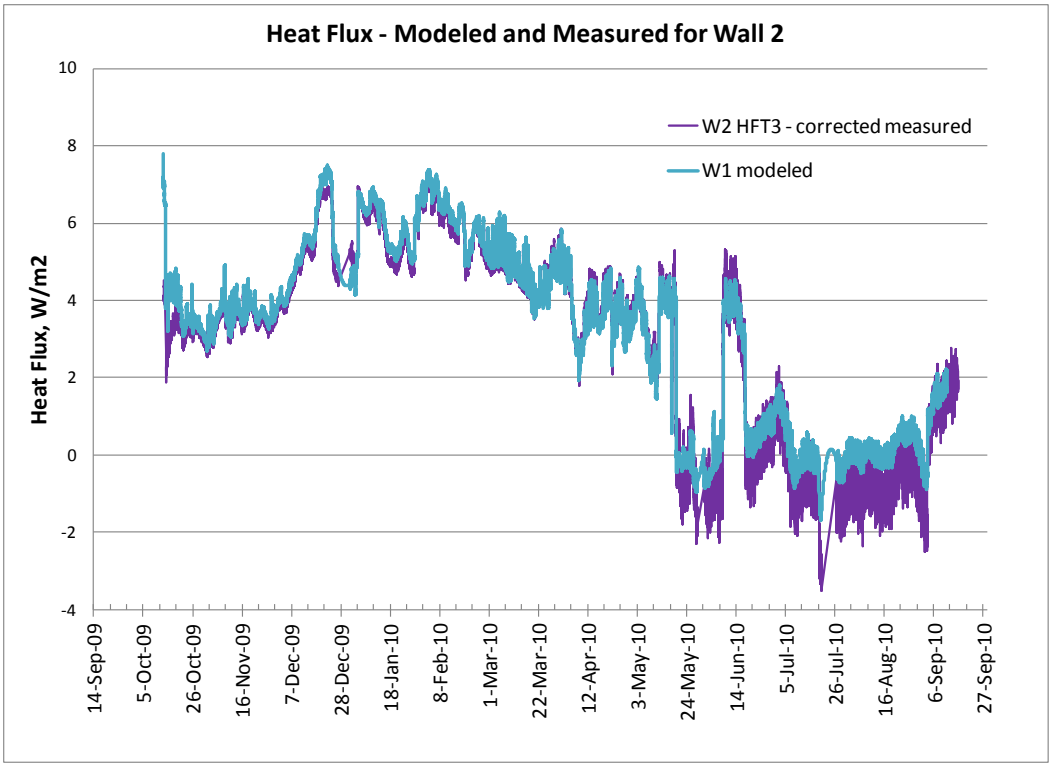

Figure 32. Comparison of the modeled heat flux and measured heat flux at location HFT3 for Wall 2.

6 Conclusions

Two ICF wall specimens were monitored at the NRC Field Exposure of Wall Facility (FEWF) from October 13th 2009 to September 16th, 2010.

In general, the measured heat flux and temperature data from the field trial revealed that the concrete added very little to the overall R-value of the ICF under steady-state conditions. The measured pseudo-steady state R-value of the ICF in this study was RSI 3.77 (R21.4).

However, during transient conditions, the data demonstrated that the concrete significantly moderated heat loss to and from the interior, providing a 5-day buffering effect. By doing so, the ICF wall was shown to reduce the 15-minute peak in heat gains to or losses from the room. The measured heating season peak in heat flux leaving the room was 8.3 W/ m^2, below the expected peak in a wall without mass effect: 10.3 W/m^2. Similarly, the peak 15-minute heat flux entering the room through the ICF in summer was 2.2 W/m^2, less than half the maximum predicted 15-minute cooling season heat gain for a wall with no mass effect (5.6 W/m^2). Thus, ICF walls have the potential to reduce the peak heating requirement of the furnace, and the peak cooling requirement of the air conditioning system. This may have implications for the sizing and cost of mechanical equipment.

Some seasonal storage effects were shown through the comparison of the total monthly measured heat loss at the interior surface of the ICF with the expected heat flux without thermal mass effect. In September, October, November and December, as the concrete cooled slowly, the average measured heat loss through the ICF was slightly less than the expected heat loss for a wall with no mass effect. The effect reversed as the concrete mass was slow to warm up from February to June. During this period, heat losses through the ICF wall are expected to be higher than heat losses for a similar wall with no mass effect. This seasonal effect was less than the impact of the mass on peak heat losses and gains.

This analysis involved comparing the measured heat losses/gain through an ICF wall to the expected heat losses/gains through a wall with no mass effect and an identical steady state R-value (RSI 3.77 [R21.4]).

The study showed the importance of the location of the sensors and especially the heat flux transducers (HFTs). Each side of the HFT should be in contact with homogeneous material. Once the positioning of the sensors was corrected, the heat flux transducers provided a good means of evaluating the performance of an ICF wall specimen. With a known R-value of the insulation in the ICF, thermocouples could also be used as an inexpensive alternative for determining heat flux analysis – this method was used to effectively predict heat flux in the first half of the experiment.

The results from this field trial were used to benchmark the NRC-IRC hygrothermal model (Saber et al., 2011). The present model will be used to conduct a parametric study in order to investigate the transient thermal response of full-scale ICF wall assemblies subjected to different cold and hot climate conditions of North America. Future work could employ this model to explore the optimization of ICF construction for different climates and wall orientations. Different thicknesses and distribution of the insulation layers could be explored as well.

This experiment only examined a small section of ICF wall on a west façade. Performance on the whole house level will be affected by other factors including solar gains through windows, and the operating mode of the house (for example: the use of free cooling at night or thermostat setbacks). Whole house modeling would be required to better understand the impact of ICF construction on annual energy consumption.

7 References

ASHRAE. 2009. *2009 ASHRAE Handbook –Fundamentals (SI)*. 26.5. Atlanta: American Society of Heating, Refrigerating, and Air-Conditioning Engineers Inc.

Enermodal. 2006. *Monitored Performance of an Insulating Concrete Form Multi-Unit Residential Building*. Final Report. Canada Mortgage and Housing Corporation. Canada. PP 1-45.

Environment Canada, 2010. *Canadian Climate Normals 1971-2000, Ottawa MacDonald Cartier International Airport* [online]. Available from: http://www.climate.weatheroffice.gc.ca [accessed 18 March 2010]

ASTM Designation: C 518-04, Steady-State Thermal Transmission Properties by Means of the Heat Flow Meter Apparatus, Section 4, Volume 04.06, Thermal Insulation, 2007 Book of ASTM Standards.

ASTM Designation: C 1130-07, "Standard Practice for Calibrating Thin Heat Flux Transducers", *Annual Book of ASTM Standards*, sec 4, Construction, vol 04.06, Thermal Insulation; Building & Environment Acoustic, pp. 577-584, 2009.

Burch, D.M., W.L. Johns, T. Jacobsen, G.N. Walton, and C.P. Reeve. 1984a. "The Effect of Thermal Mass on Night Temperature Setback Savings." *ASHRAE Transactions,* 90(part 2), 184-206.

Burch, D.M., K.L. Davis, and S.A. Malcomb. 1984b. "The Effect of Wall Mass on the Summer Space Cooling of Six Test Buildings." *ASHRAE Transactions* 90 (part 2), 5-21.

Burch, D.M., D.F. Krintz, and R.F. Spain. 1984c. "The Effect of Wall Mass on Winter Heating Loads and Indoor Comfort—An Experimental Study." *ASHRAE Transactions* 90 (part 1), 94-114.

Christian, J.E. 1991. "Thermal Mass Credits Relating to Building Energy Standards." *ASHRAE Transactions* 97 (part 2), 941-957. Christian, J.E., J. Kosny, A.O. Desjarlais, and P.W. Childs. 1998. "The Whole Wall Thermal Performance Calculator–On the Net." In *Proceedings, Thermal Performance of the Exterior Envelopes of Buildings VII,* 287-299. Atlanta, Ga.: American Society of Heating, Refrigerating and Air-Conditioning Engineers.

Elmahdy, A.H., Maref, W., Swinton, M.C., Saber, H.H., and Glazer, R. 2009-b. Development of energy ratings for insulated wall assemblies. Building Envelope Symposium, San Diego, California, October 26, 2009, pp. 21-30.

Gajda, J., 2001. *Energy Use of Single-Family Houses with Various Exterior Walls*. Research & Development Information Report. Portland Cement Association and Concrete Foundations Association. PCA CD026. PP 1-46.

Hersh Servo AG. 2010. *Insulated Concrete Forms* [online]. Available from: http://www.hirsch-gruppe.com [accessed 29 April 2010]

Enermodal, *Monitored Performance of an Insulating Concrete Form Multi-Unit Residential Building*, Draft Final Report, prepared by Enermodal Engineering Limited, www.enermodal.com, September 2006.

Kosny, J., E. Kossecka, A.O. Desjarlais, and J.E. Christian. 1998. "Dynamic Thermal Performance of Concrete and Masonry Walls." In *Proceedings, Thermal Performance of the Exterior Envelopes of Buildings VII,* 629-643. Atlanta, Ga.: American Society of Heating, Refrigerating and Air-Conditioning Engineers.

Kosny, J., T. Petrie, D. Gawin, P. Childs, A. Desjarlais and J. Christian. 2001. "Energy Benefits of Application of Massive Walls in Residential Buildings." In *Proceedings, Performance of Exterior Envelopes of Whole Buildings VIII,* Session IX-A. Atlanta, Ga.: American Society of Heating, Refrigerating and Air-Conditioning Engineers.

Kossecka, E., and J. Kosny. 1998. "Effect of Insulation and Mass Distribution in Exterior Walls on Dynamic Thermal Performance of Whole Buildings." In *Proceedings Thermal Performance of the Exterior Envelopes of Buildings VII*, 721-731. Atlanta, Ga.: American Society of Heating, Refrigerating and Air-Conditioning Engineers.

NAHB Research Center 1999, "Insulating Concrete Forms: Comparative Thermal Performance" prepared for U.S. Dept. of Housing and Urban Development. August 1999.

Petire, T., Kosny, J., Desjarlais, A., Atchley, J., Childs, P.W., Ternes, M.P. and Christian, J., 2001, "How Insulating Concrete Form vs. Conventional Construction of Exterior Walls Affects Whole Building Energy Consumption: Results from a Field Study and Simulation of Side-by-Side Houses"

Rabin, Y., and Rittel, D. "A Model for the Time Response of Solid-embedded Thermocouples", *Experimental Mechanics,* VoL 39, No. 2, pp. 132-136, 1999.

Saber, H.H., et al. 2010a. 3D Thermal Model for Predicting the Thermal Resistances of Spray Polyurethane Foam Wall Assemblies. *Proceedings of Thermal Performance of the Exterior Envelopes of Whole Buildings XI International Conference*. Clearwater, Florida. December 5-9, 2010.

Saber, H.H., et al. 2010b. 3D Thermal Model for Predicting the Thermal Response of Insulating Concrete Form (ICF) Wall. *Proceedings of Thermal Performance of the Exterior Envelopes of Whole Buildings XI International Conference*. Clearwater, Florida. December 5-9, 2010.

Saber, H.H. et al. 2011. *Numerical Simulations to Predict the Thermal Response of Insulating Concrete Form (ICF) Wall in Cold Climate*. Nov, 2011. National Research Council Canada. RR-310.

Appendix A - ICF Construction

Preparing the FEWF site for ICF installation

Figure A-1. Removal of trees from the FEWF site, allowing full west exposure to wind, rain and sun.

Figure A-2. Installation of a gravel pad to allow the forklift room to manoeuvre when lifting the ICF walls into place.

ICF Assembly

Figure A-3. Assembling the insulating form inside the Research House.

Figure A-4. Three assembled insulating forms inside the Research House. Note: three ICF wall specimens were fabricated, although only two were installed for monitoring at the FEWF. The third wall was made as a backup, in case either of the other two wall specimens was damaged during installation.

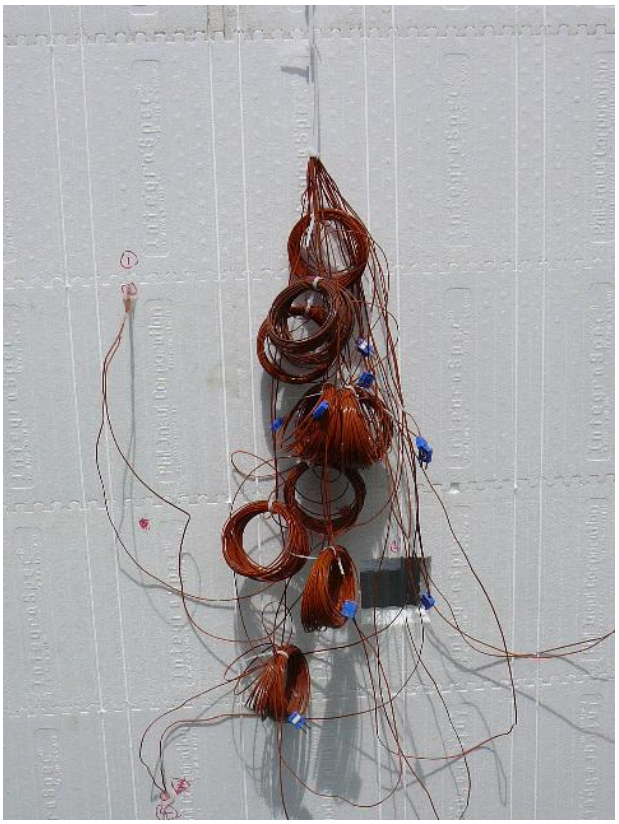

Figure A-5. Thermocouples installed on the exterior and interior surfaces of the foam prior to pouring the concrete.

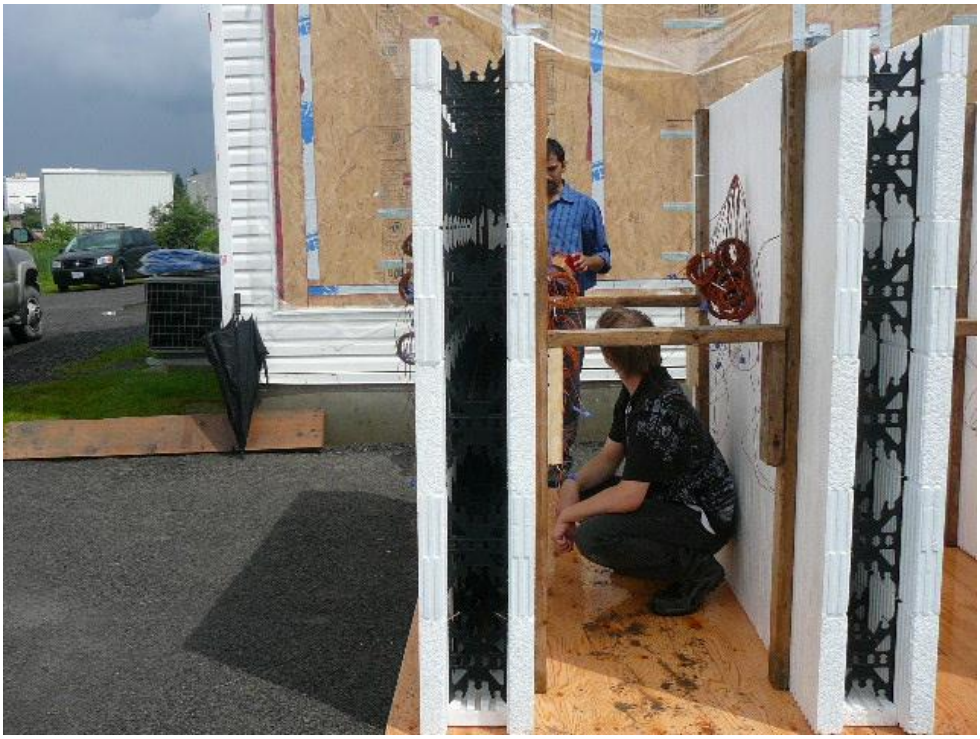

Figure A-6. Preparing the three insulating forms for the concrete pour.

Figure A-7. Steel rebar inserted into the ICF frame prior to pouring the concrete.

Figure A-8. Preparing the three insulating forms for the concrete pour.

Pouring the concrete – July 28th, 2009

Figure A-9. Preparing the three insulating forms for the concrete pour.

Figure A-10. Arrival of the concrete mixer and pumping truck.

Figure A-11. Pouring the concrete into the insulating form.

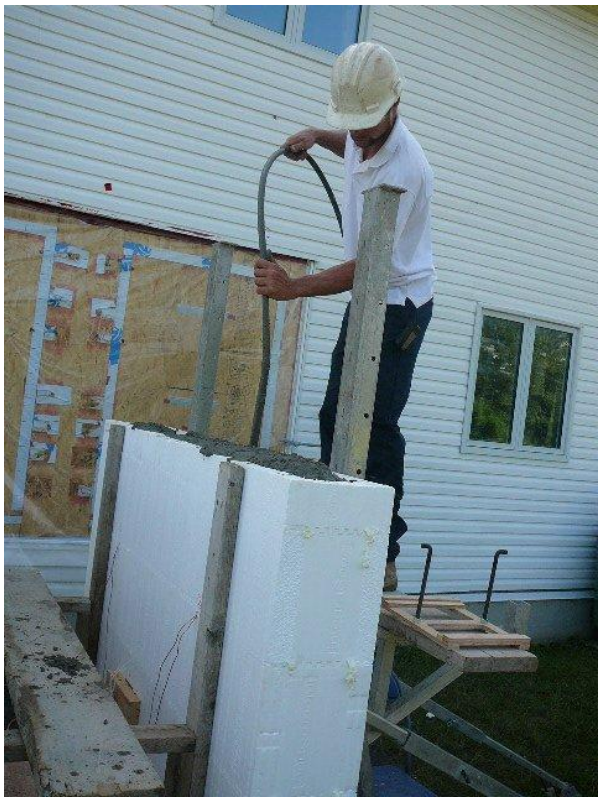

Figure A-12. Vibrating the concrete to remove air pockets.

Figure A-13. Water pooling at the base of the ICF wall specimen after pouring the concrete.

Figure A-14. Water pooling at the base of the ICF wall specimen after pouring the concrete.

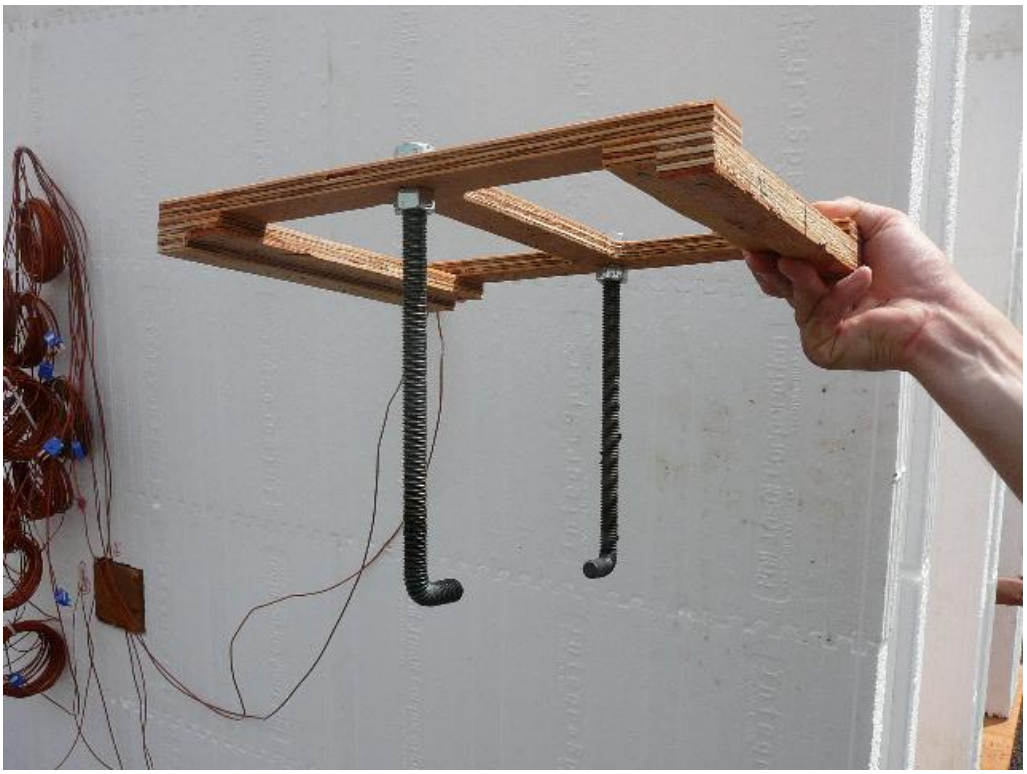

Figure A-15. Wooded alignment jig with threaded rods for the forklift lifting points.

Figure A-16. The alignment jig holds the metal rods in place while the concrete cures.

Figure A-17. Once the concrete was cured, the wooded jig was removed, extensions were added to the threaded rods, and metal plates were attached to provide lifting points for the forklift.

ICF Installation – August 25th, 2009 (after 28 days of curing)

Figure A-18. Preparing the FEWF opening for ICF wall installation.

Figure A-19. Preparing the FEWF opening for ICF wall installation.

Figure A-20. Lifting the first ICF wall into position.

Figure A-21. Lifting the first ICF wall into position.

Figure A-22. The ICF is separated from the framing by 4 inches of EPS foam on the sides, bottom and top (not shown).

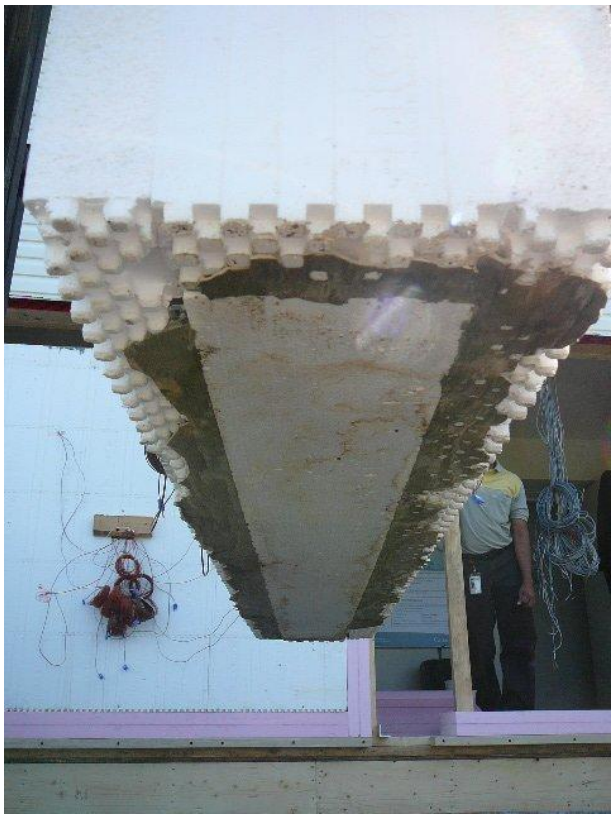

Figure A-23. View of the bottom of the second ICF wall specimen as it is being lifted into position.

Figure A-24. Lifting the second ICF wall specimen into position.

Figure A-25. Lifting the second ICF wall specimen into position.

Figure A-26. Securing the second ICF wall specimen.

Figure A-27. Securing the second ICF wall specimen. Temporary vertical wood straps help guide the ICF wall specimen into place in the FEWF opening.

Figure A-28. ICF wall specimens installed in the FEWF opening.

Figure A-29. Metal L brackets hold the framing in place on either side of the ICF.

Figure A-30. Metal L brackets hold the framing in place on either side of the ICF.

Figure A-31. Metal L brackets hold the framing in place on either side of the ICF.

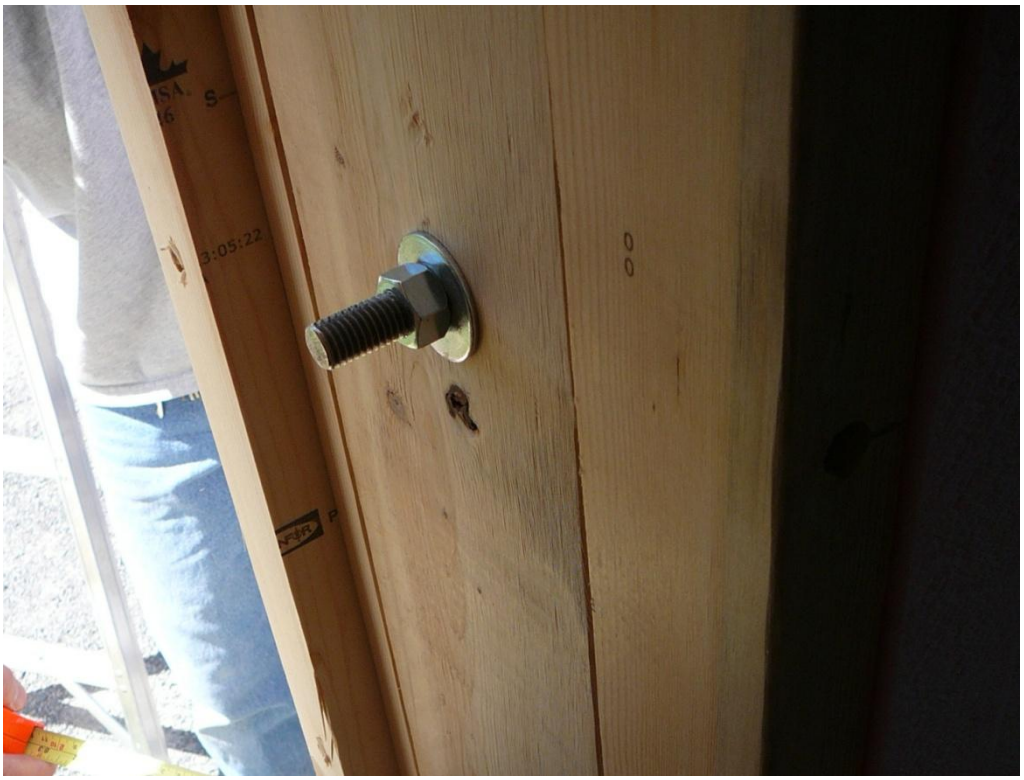

Figure A-32. Bolts secure the ICF wall specimen to the wood framing (2 bolts on each side).

Finishing details – Exterior

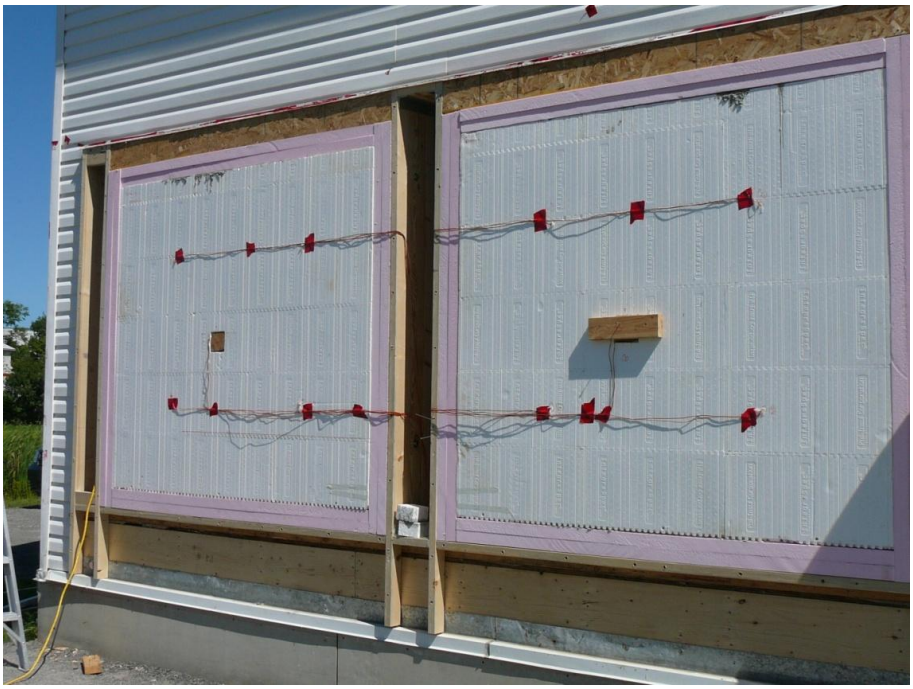

Figure A-33. Instrumentation installed on the exterior of the walls, wires run to the chase between the two ICF specimens.

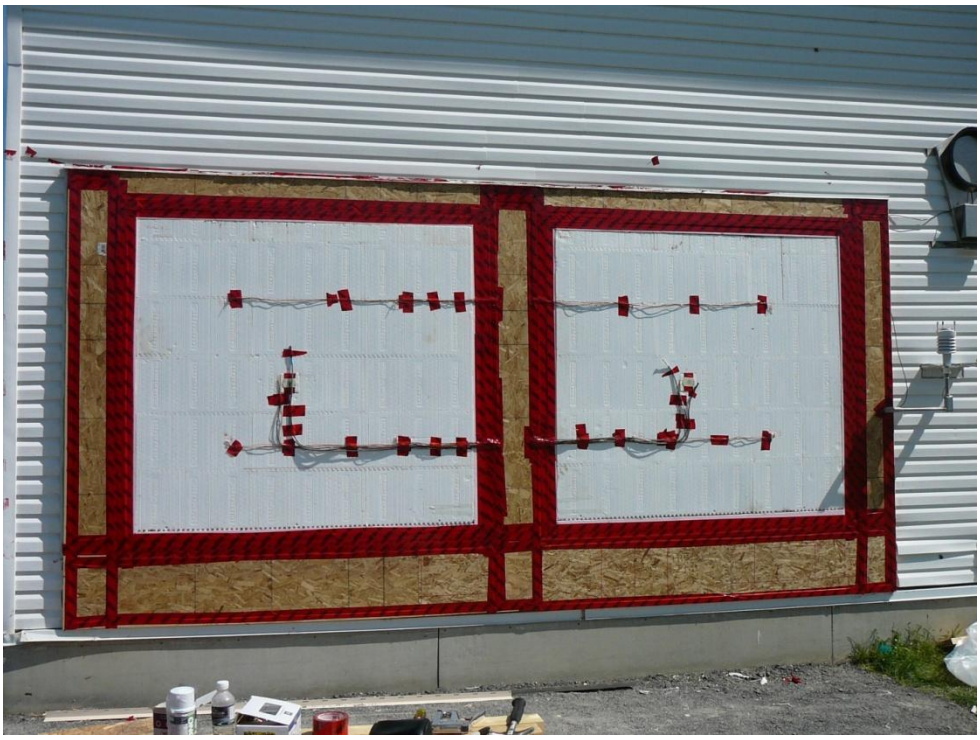

Figure A-34. OSB sheathing board installed around the specimens, joints sealed with sheathing tape.

Figure A-35. Sheathing membrane installed over the sheathing board, and cut to expose the face of the ICF walls. Sheathing membrane taped to the ICF on all four sides (shown in subsequent figures).

Figure A-36. Gaps in the ICF foam filled with low expansion polyurethane foam. A temporary sheathing membrane skirt prevents foam from adhering to the permanent sheathing membrane.

Figure A-37. Gaps in the ICF foam filled with low expansion polyurethane foam. A temporary sheathing membrane skirt prevents foam from adhering to the permanent sheathing membrane.

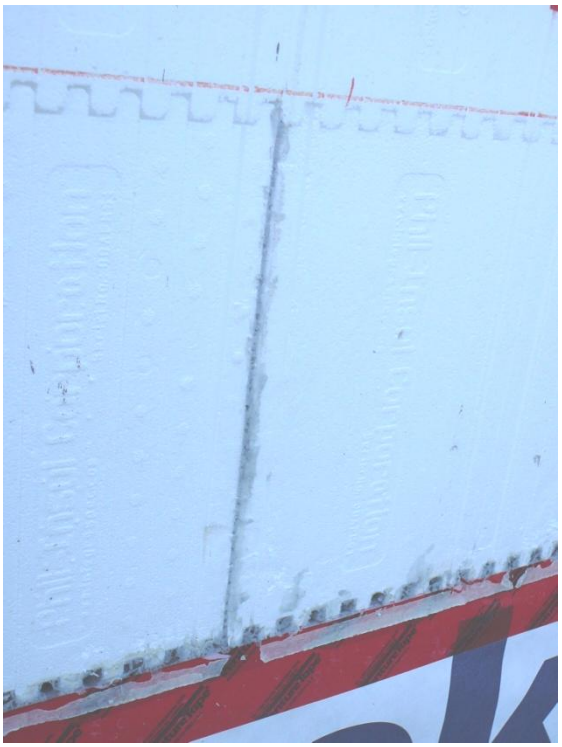

Figure A-38. Excess foam trimmed from the face of the ICF once cured, with the temporary skirt removed.

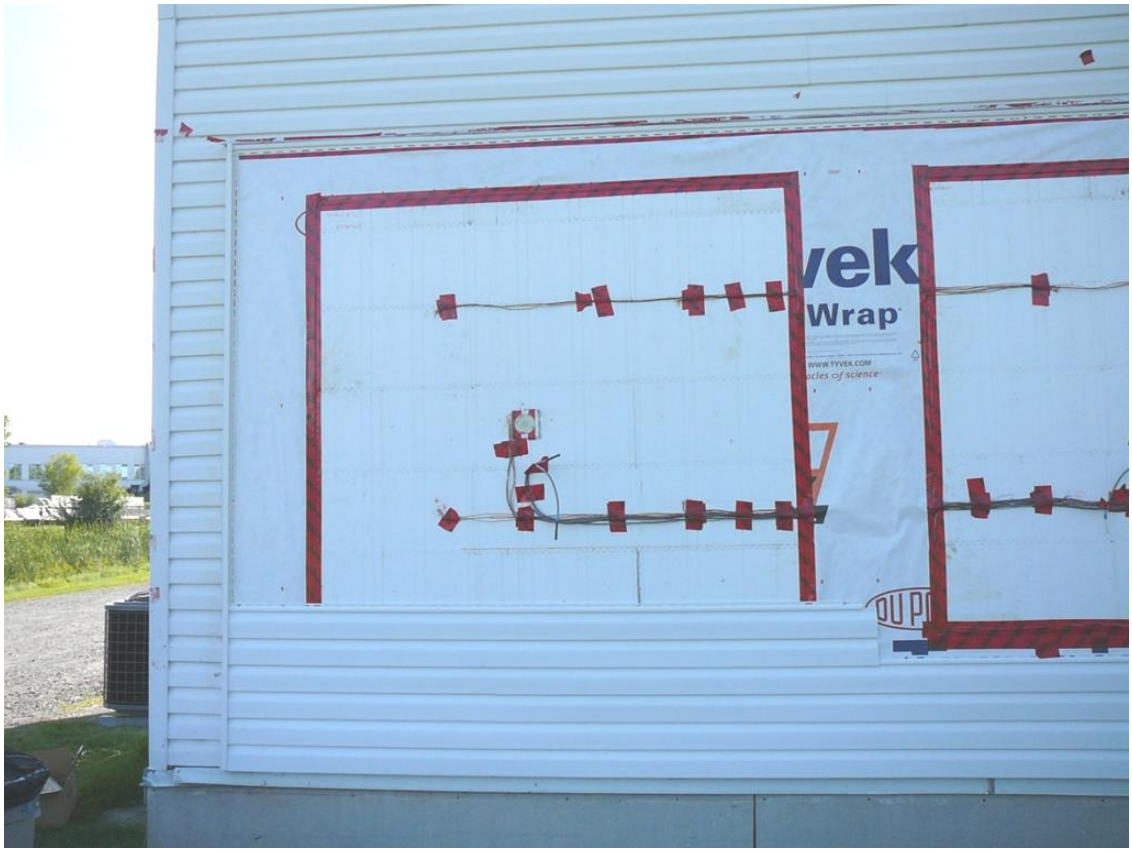

Figure A-39. Installation of vinyl siding over the entire FEWF opening.

Figure A-40. Detail view of instrumentation behind the vinyl siding – including: a heat flux transducer (round disk), pressure tap (clear plastic tube), and RH&T sensor (black sensor).

Finishing details – Interior

Figure A-41. Gaps in the ICF foam filled with low expansion polyurethane foam. Once cured, excess foam was trimmed from the interior face of the ICF.

Figure A-42. Instrumentation secured to the interior face of the ICF wall.

Figure A-43. Drywall being installed on the interior of the ICF wall specimens. A square access panel was cut in the centre of the drywall to allow access to the instrumentation (including heat flux transducers) on the surface of the ICF.

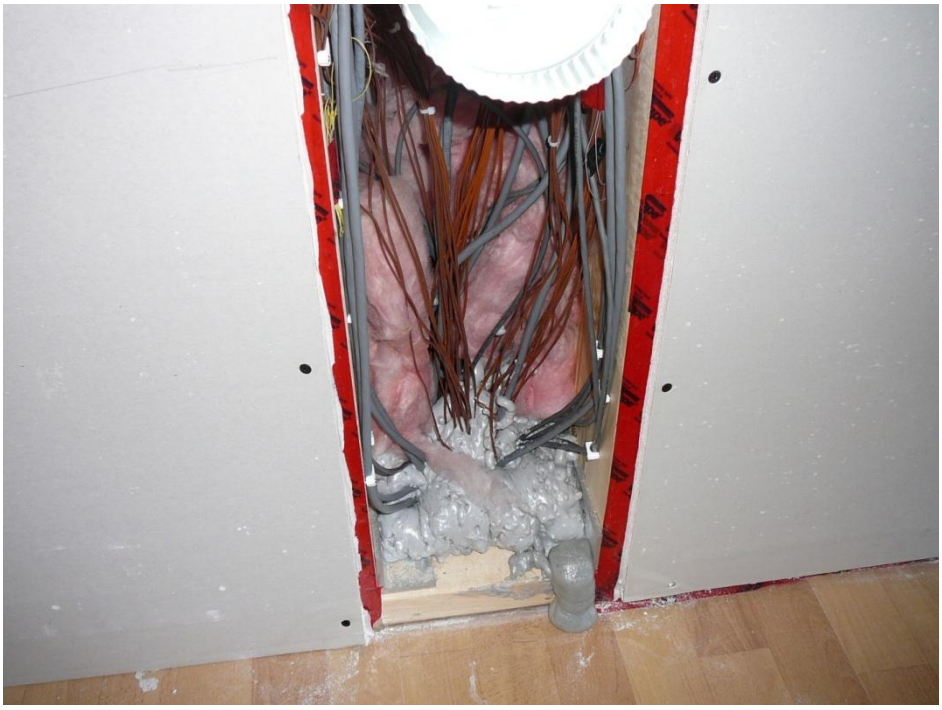

Figure A-44. Wiring in the chase between the ICF walls leads to the basement. The holes for the wiring to pass through the base plate were sealed with foam.

Figure A-45. The wiring chase was filled with glass fibre batt insulation, and sealed with a polyethylene air/vapour barrier.

Figure A-46. Tape seals the air/vapour barrier to the surrounding wall assembly. A ventilation duct passes through the wiring chase, to permit air conditioning of the test chamber during the cooling season.

Figure A-47. Installing drywall over the wiring chase between the ICF walls.

Figure A-48. Covering the seams and screw holes with drywall compound.

Figure A-49. The seams and screw holes in the wall covered with drywall compound.

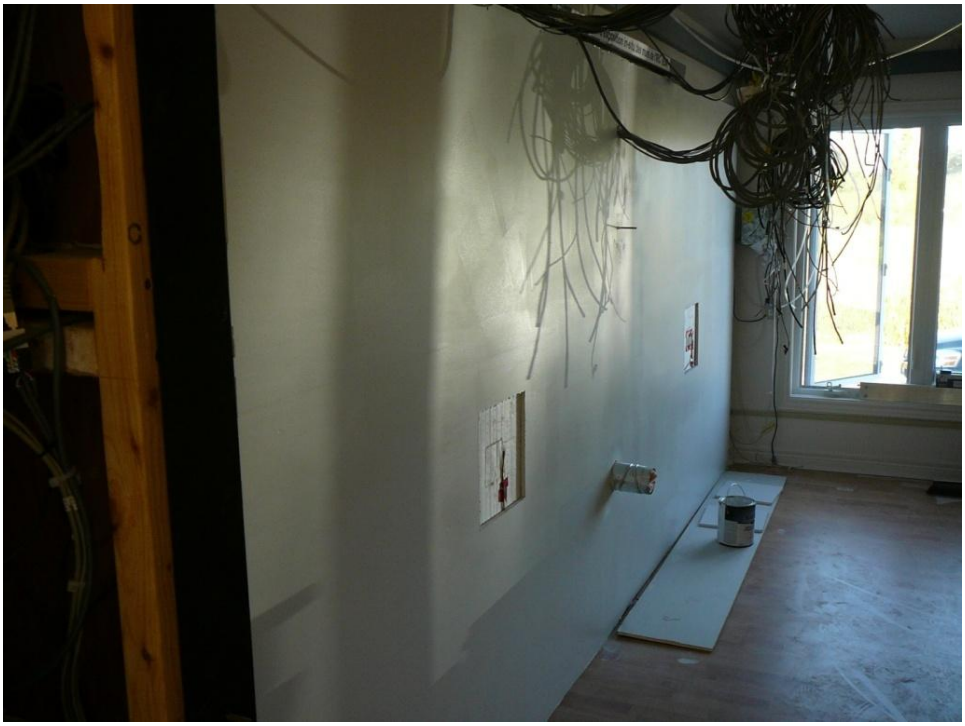

Figure A-50. ICF walls painted with acrylic paint – with access panels open (the removed sections of drywall were set back into place and taped before the start of the experiment)

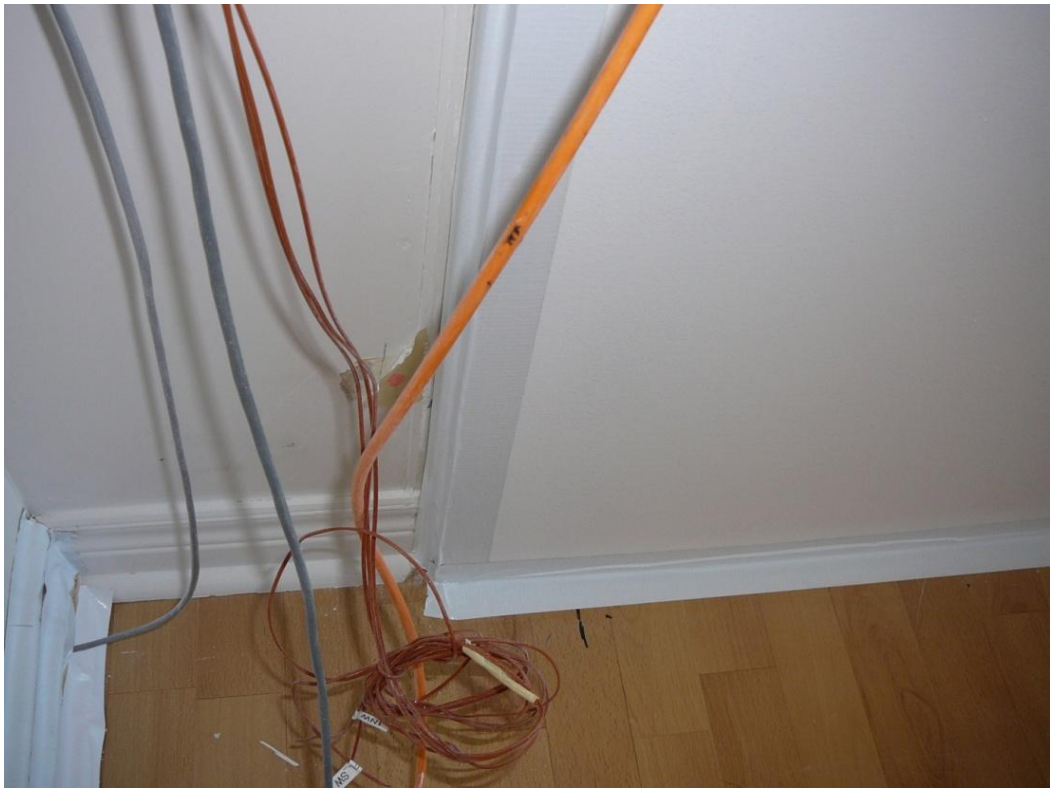

Figure A-51. The edges of the drywall were taped to the surrounding walls, floor and ceiling.

Figure A-52. Installation of the interior climate control chamber.

Figure A-53. Installation of the interior climate control chamber.

Heat Flux Sensors

Figure A-54. Removing a block of the EPS foam from the insulating form.

Figure A-55. Removing a block of the EPS foam from the insulating form.

Figure A-56. Replacing the foam block with a piece of wood for the concrete pour.

Figure A-57. Filling the ridges of the foam blocks with concrete.

Figure A-58. Filling the ridges of the foam blocks with concrete.

Figure A-59. Curing the concrete in controlled conditions.

Figure A-60. The foam blocks with cured concrete, prior to installation into the ICF walls.

Figure A-61. Cured ICF wall with removed foam block.

Figure A-62. Positioning of a heat flux transducer on the surface of the concrete.

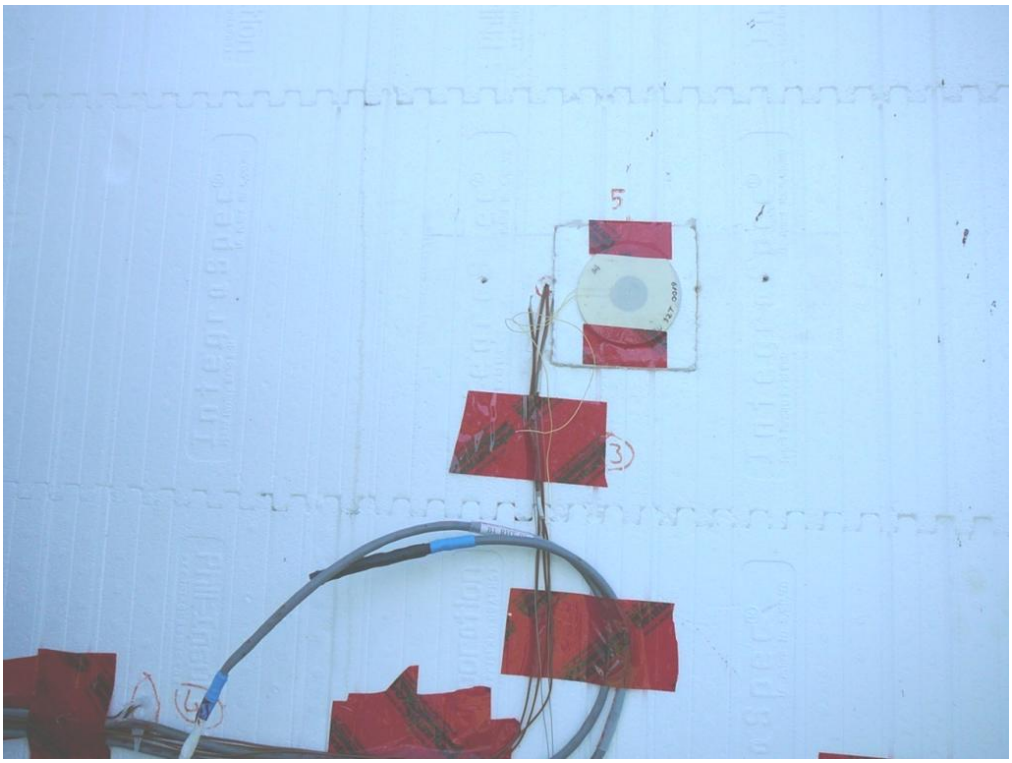

Figure A-63. Re-installation of the foam block, with a second heat flux transducer installed on the outer surface of the EPS.

Repositioning the Heat Flux Transducers

Figure A-64. Removal of the heat flux transducer on the surface of the concrete, for repositioning.

Figure A-65. Foam blocks cut into two.

Figure A-66. Repositioning of the heat flux centre between the two sections of the foam block.

Figure A-67. Installing the foam block back in the ICF wall.

Figure A-68. Installing a second heat flux transducer on the interior surface of the ICF.

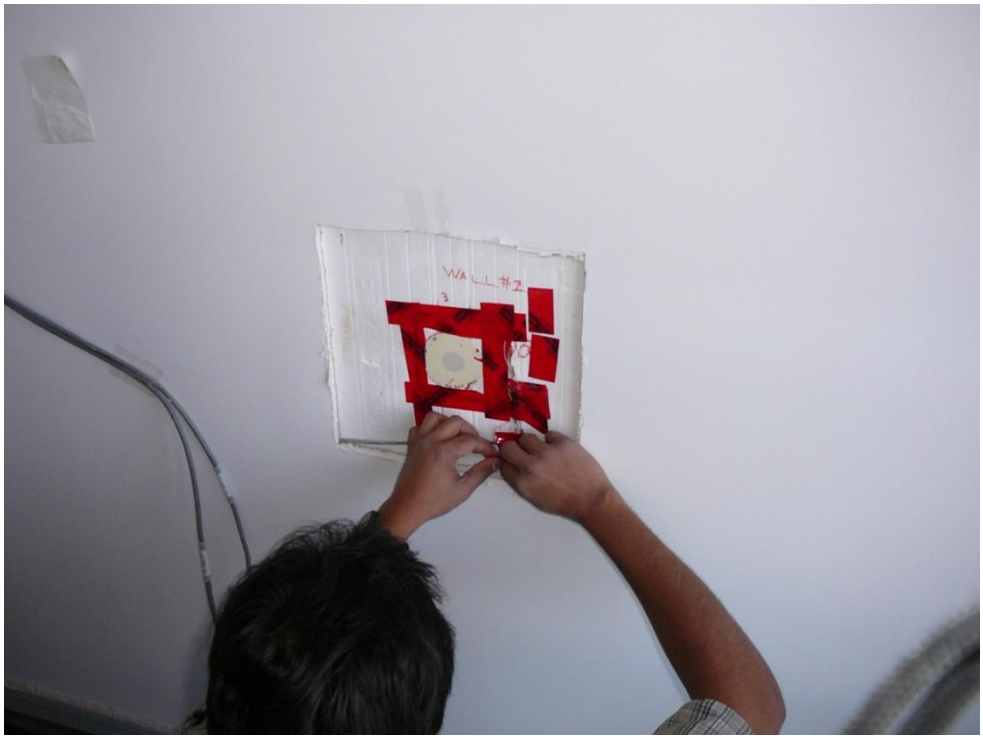

Figure A-69. Sealing the edges of the foam block to the ICF with tape.

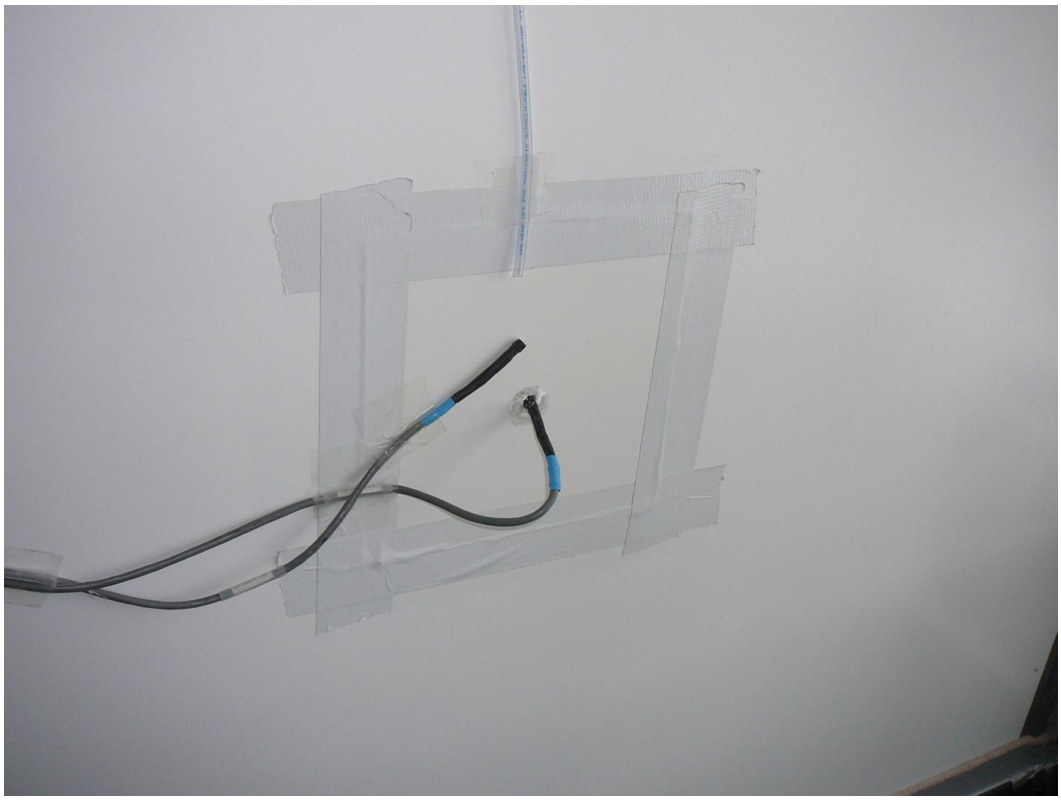

Figure A-70. Installation of the drywall access panel on top of the heat flux transducer, and repositioning of instrumentation (2 RH&T sensors and one pressure tap are shown).